




Hypothalamic-hindbrain circuit for consumption-induced fear regulation

Received: 22 December 2023

Accepted: 21 August 2024

Published online: 04 September 2024

 Check for updatesQin Wang ^{1,6}, Rui-Yue Sun^{1,6}, Jia-Xue Hu¹, Yan-Hui Sun¹, Chun-Yue Li¹, Huiqian Huang¹, Hao Wang ^{1,2,3} ✉ & Xiao-Ming Li ^{1,2,4,5} ✉

To ensure survival, animals must sometimes suppress fear responses triggered by potential threats during feeding. However, the mechanisms underlying this process remain poorly understood. In the current study, we demonstrated that when fear-conditioned stimuli (CS) were presented during food consumption, a neural projection from lateral hypothalamic (LH) GAD2 neurons to nucleus incertus (NI) relaxin-3 (RLN3)-expressing neurons was activated, leading to a reduction in CS-induced freezing behavior in male mice. LH^{GAD2} neurons established excitatory connections with the NI. The activity of this neural circuit, including NI^{RLN3} neurons, attenuated CS-induced freezing responses during food consumption. Additionally, the lateral mammillary nucleus (LM), which received NI^{RLN3} projections, along with RLN3 signaling in the LM, mediated the decrease in freezing behavior. Collectively, this study identified an LH^{GAD2}-NI^{RLN3}-LM circuit involved in modulating fear responses during feeding, thereby enhancing our understanding of how animals coordinate nutrient intake with threat avoidance.

Survival requires organisms to balance nutrient intake with danger avoidance, necessitating adaptive behaviors. The drive for energy acquisition motivates feeding behaviors, potentially exposing organisms to threats that induce fear. In humans, abnormal patterns of food consumption are often linked to psychiatric disorders involving fear and anxiety^{1–3}. While this suggests that food consumption may sometimes regulate fear, the mechanisms underlying this phenomenon remain unclear.

As a motivational behavior, feeding encompasses both appetitive and consummatory actions. The need for energy triggers the desire for food, promoting appetitive behaviors, such as food seeking, encoded by agouti-related peptide (AgRP) neurons of the arcuate nucleus (Arc)^{4,5}. Once food is available, appetitive behaviors are replaced by consummatory behaviors. Previous research has implicated the lateral hypothalamus (LH) in the control of feeding and regulation of various

reward and aversion-related behaviors^{6–9}. The complex functions of the LH stem from its heterogeneous cell population¹⁰. During feeding, GABAergic neurons in the LH are activated, promoting food consumption^{11,12} and encoding reward behaviors^{13,14}. In contrast, LH glutamatergic neurons induce aversion behaviors when activated, inhibiting food consumption⁷. A critical question therefore arises: how do LH neurons respond to and regulate conflicting feeding and fear behaviors when an animal encounters dangerous stimuli during food consumption?

Previous studies have demonstrated that fear and stress can suppress feeding-related behaviors^{15,16}, involving multiple parallel neural circuits in the brain^{17–20}. While fear generally inhibits food consumption, it is conceivable that feeding behaviors driven by caloric need could, in turn, regulate fear responses. Research has shown that while predator stimulation reduces food seeking and consumption in

¹Department of Neurobiology and Department of Psychiatry of the Second Affiliated Hospital, Zhejiang University School of Medicine, Hangzhou, China.

²Nanhu Brain-computer Interface Institute, Hangzhou, China. ³Affiliated Mental Health Center and Hangzhou Seventh People's Hospital, Zhejiang University School of Medicine, Hangzhou, China. ⁴NHC and CAMS Key Laboratory of Medical Neurobiology, MOE Frontier Science Center for Brain Science and Brain-machine Integration, School of Brain Science and Brain Medicine, Zhejiang University, Hangzhou, China. ⁵Center for Brain Science and Brain-Inspired Intelligence, Research Units for Emotion and Emotion Disorders, Chinese Academy of Medical Sciences, Hangzhou, China. ⁶These authors contributed equally: Qin Wang, Rui-Yue Sun. ✉ e-mail: wanghao890625@126.com; lixm@zju.edu.cn

hungry rats, increased caloric need antagonizes this effect via projections from AgRP neurons to the bed nucleus of the stria terminalis (BNST) and/or LH²¹. Photogenetic activation of AgRP neurons augments feeding while attenuating anxiety-related behaviors and fear^{22–24}. Two groups of LH neurons, expressing leptin receptors and neurotensin, respectively, have been reported to competitively regulate conflicting demands for social interaction, food, and water²⁵. Overall, these findings suggest that the hypothalamus, particularly the LH, is a crucial brain region for processing conflicting responses to feeding and fear.

The hindbrain is also critical in controlling feeding. Research has shown that glutamatergic neurons in the peri-locus coeruleus (periLC) control motivation for food and water consumption²⁶, while the nucleus incertus (NI) is involved in arousal²⁷, stress^{28,29}, and stressor-associated motivated ingestion behaviors^{30,31}, with relaxin-3 (RLN3)-expressing neurons and their ascending RLN3/relaxin-family peptide receptor 3 (RXFP3) playing a key role³². The NI and RLN3/RXFP3 system have also been implicated in the regulation of anxiety^{33,34} and fear^{27,35,36}. These studies suggest that the NI and RLN3/RXFP3 system may be key centers in the hindbrain for processing various conflicting information.

Given the potential role of the LH and hindbrain in regulating food consumption-related fear, we identified a circuit extending from the LH to the hindbrain that is instrumental in mediating consumption-induced regulation of learned freezing responses.

Results

Consumption-induced freezing regulation with LH^{GAD2} involvement

To examine the modulation of learned freezing responses during food consumption, we developed a fear-feeding assay (Fig. 1a). Initially, in the pretest sessions, mice were exposed to a conditioned stimulus (CS)—a neutral sound—while having unrestricted access to food. During the conditioning session, the CS was paired with a footshock, serving as the unconditioned stimulus (US). During the post-test session, the mice were divided into three distinct groups. The fed-food and fasted-food mice were subjected to the CS with unrestricted access to food, either in a state of satiation or fasting, respectively. In contrast, fasted-no food mice were exposed to the CS in a fasted state without access to food. Comparative analysis revealed that, in contrast to the fed-food mice, the fasted-food mice exhibited a substantial reduction in CS-induced freezing responses (Fig. 1b). Additionally, fasted-food mice showed a significant decrease in eating time during CS in the post-test session ($-29.32\% \pm 3.85\%$) compared to baseline (BS, $-9.00\% \pm 3.12\%$; Supplementary Fig. 1a). Notably, although CS generally inhibited feeding in the post-test session and completely suppressed it during the first CS, there was a slight recovery of consummatory behavior during subsequent CSs, accompanied by a marked decline in learned freezing responses (Supplementary Fig. 1b). These results suggest that food consumption can adaptively regulate learned freezing responses, although this regulation is not a direct antagonistic effect of feeding behavior on freezing.

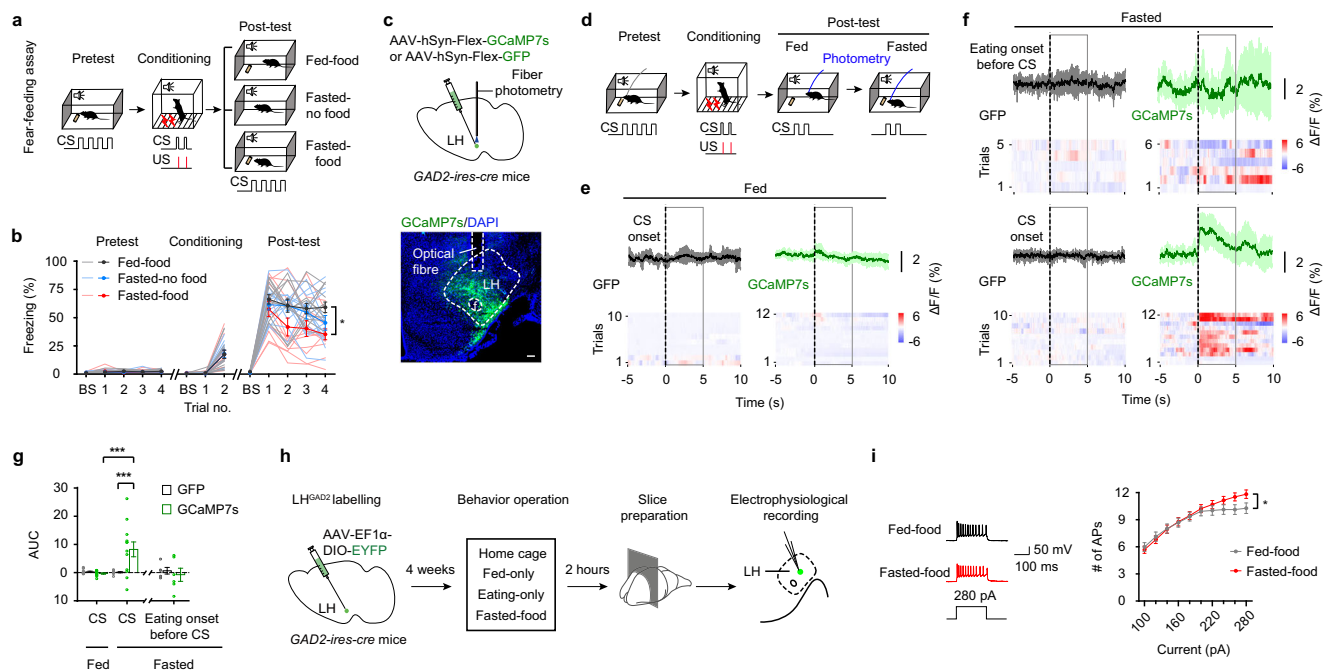


Fig. 1 | Consumption-induced freezing regulation with LH^{GAD2} involvement.

a Schematic of fear-feeding assay. CS conditioned stimulus, US unconditioned stimulus. **b** Assessment of freezing responses at baseline (BS) and during CSs for each session of the fear-feeding assay, $n = 12$ mice/group, dark- and light-colored lines each represent average and individual, respectively. **c** Schematic representing LH^{GAD2} GCaMP recordings with representative image indicating locations of GCaMP transduction and optical fibers. Scale bar, 100 μm . **d** Experimental design outlining LH^{GAD2} fiber photometry. Traces and heat maps from LH^{GAD2} fiber photometry in GFP- or GCaMP7s-injected mice responding to CS under fed (**e**) and fasted (**f**, bottom) states, and beginning to feed before CS presentation (**f**, top). The normalized change in fluorescence ($\Delta F/F$) was calculated. Black dashed lines at time 0 denote CS or eating onset. Black and green solid lines indicate average fluorescence traces, while shadings represent 95% confidence interval. **g** Mean area under the curve (AUC) from LH^{GAD2} fiber photometry responses to CS and eating

onset. Data were extracted within a 5-s window following CS presentation or eating onset (gray frame in (**e**, **f**)). **e–g** $n = 10$ trials/5 GFP mice, 12 trials/6 GCaMP7s mice for CSs; $n = 5$ trials/5 GFP mice, 6 trials/6 GCaMP7s mice for eating onset.

h Schematics of EYFP labeling and neuronal recordings of LH^{GAD2} neurons.

i Representative traces showing firing responses to a 280-pA current injection (left) and number of action potentials (AP; right) evoked by step current injection (100–280 pA with a 20-pA step) in LH^{GAD2} neurons, $n = 40$ neurons/3 mice per group. Data were presented as the mean \pm SEM; * $p < 0.05$, *** $p < 0.001$. Statistical significance was assessed using two-way repeated measures (RM) ANOVA with Tukey's multiple-comparisons tests (**b**) or uncorrected Fisher's least significant difference (LSD) multiple-comparisons test (for CS in (**g**)), two-sided unpaired t -test (for eating onset before CS in (**g**)) or two-way RM ANOVA (**i**). Source data and exact p value are provided as a Source Data file.

Given that distinct subpopulations of LH neurons are responsible for encoding feeding and aversion-related behaviors, we first examined which types of LH neurons were activated in the fear-feeding assay. Following the post-test session, the gene expression levels of *Fos*, *Slc17a6* (encoding vesicular glutamate transporter 2 (VgluT2), a marker for glutaminergic neurons), and *Slc32a1* (encoding vesicular GABA transporter (Vgat), a marker for GABAergic neurons) in the LH cells were assessed by RNAscope in situ hybridization. *Fos* gene analysis revealed a significant increase in LH activity of fasted-food mice compared to fed-food and fasted-no food mice, with a notable increase in the number of *GAD2*-positive or *GAD2/Slc17a6* double-positive cells expressing *Fos* (Supplementary Fig. 2a–e). Similarly, a significant increase in the number of *Slc32a1*-positive LH cells expressing *Fos* was observed, with nearly all these cells also exhibiting *GAD2* gene expression (Supplementary Fig. 2f–j). Correspondingly, there was a significant increase in the proportion of *Fos*-expressing cells within *GAD2*-positive LH cells (Supplementary Fig. 2k). In the LH, most *GAD2*-positive cells co-expressed *Slc32a1* ($83.51\% \pm 2.65\%$), with a small portion co-expressing *Slc17a6* ($5.62\% \pm 1.19\%$) or *Slc32a1* and *Slc17a6* ($2.73\% \pm 0.23\%$) (Supplementary Fig. 2l, m). Nearly all *Slc32a1*-positive cells in the LH expressed *GAD2* ($98.83\% \pm 0.47\%$) (Supplementary Fig. 2l, n). These results suggest that CS presentation during food consumption activates a subgroup of *GAD2* neurons in the LH, most expressing *Slc32a1* and a small fraction expressing *Slc17a6*.

Considering the observed changes in the number of *GAD2* neurons expressing *Fos* following the fear-feeding assay, we hypothesized that LH^{GAD2} neurons likely play an important role in fear regulation during food consumption. To test this, we recorded GCaMP signals from LH^{GAD2} neurons (Fig. 1c) while conditioned mice were exposed to CSs in both fed and fasted states, with unrestricted access to food (Fig. 1d). Results revealed no significant changes in LH^{GAD2} GCaMP activity when fed mice responded to CSs or when fasted mice began consuming food prior to CS presentation. However, an increase in LH^{GAD2} GCaMP activity was observed when fasted mice were exposed to CSs during food consumption (Fig. 1e–g; Supplementary Fig. 3a, b). Large fluctuations in GCaMP responses were detected during the first eating onset before CS in fasted mice, possibly due to the heterogeneous activity of GABA neurons in the LH as mice transitioned from a starvation to food consumption state^{11,12}. Notably, a marked increase in LH^{GAD2} GCaMP activity was noted when fasted mice resumed eating post-CS presentation (Supplementary Fig. 3c–f). These findings suggest that LH^{GAD2} neurons are selectively recruited for response to CSs during food consumption.

Fos gene analysis also revealed that most *Fos*-expressing LH neurons were *Slc17a1*-positive, although their numbers did not differ significantly among the three groups. To examine the activity of LH^{VgluT2} neurons during the fear-feeding assay, we recorded GCaMP signals of LH^{VgluT2} neurons (Supplementary Fig. 3g) in conditioned mice exposed to CSs in both fed and fasted states, with unrestricted access to food. Results indicated a significant elevation in LH^{VgluT2} GCaMP activity when fed mice responded to CSs, with an even stronger GCaMP response when fasted mice were exposed to CSs during food consumption (Supplementary Fig. 3h–k). This increase in GCaMP signals likely due to additional activation of LH^{VgluT2} neurons, co-expressing *GAD2*, as hinted by above-mentioned *Fos* gene analysis. Conversely, when fasted mice began consuming food prior to CS presentation, LH^{VgluT2} GCaMP activity decreased, with this effect becoming weaker when fasted mice resumed eating post-CS presentation (Supplementary Fig. 3l–o). These results suggest that most LH^{VgluT2} neurons respond to aversive CS and are less active during food consumption, indicating a distinct activity pattern compared to LH^{GAD2} neurons.

To determine how food consumption influences the response of LH^{GAD2} neurons to CSs at the cellular level, ex vivo brain slice recordings were employed to assess the electrophysiological properties of LH^{GAD2} neurons following the fear-feeding assay. Initially, these

neurons were labeled with EYFP, after which the mice were subjected to fear conditioning and divided into four distinct groups: fed-food, fasted-food, eating-only, and home cage control (Supplementary Fig. 4a, “Methods” section). The eating-only group consisted of mice that consumed food in a fasted state without CS exposure, while the home cage group served as the control. At 2 h post-behavioral manipulation, whole-cell recordings of EYFP-marked LH^{GAD2} neurons were conducted (Fig. 1h). Measurements of resting membrane potential (RMP) and input resistance (R_{in}) revealed no significant differences among the four groups of EYFP-positive neurons (Supplementary Fig. 4b, c). Depolarizing current injections (0–100 pA with a 5-pA step) were then employed to evaluate the action potential (AP) threshold. Compared to control neurons, EYFP-positive neurons from the eating-only and fasted-food group showed a lower AP threshold current (Supplementary Fig. 4d). Further assessment of neuronal excitability using a larger current injection (100–280 pA with a 20-pA step) revealed that EYFP-labeled neurons in the eating-only group elicited more APs than those in the control group (Supplementary Fig. 4e). Similarly, neurons from the fasted-food group displayed a higher number of APs compared with those in the fed-food group (Fig. 1i). These findings suggest that food consumption enhances the excitability of LH^{GAD2} neurons, significantly increasing their activity post-CS presentation. Thus, the heightened excitability induced by food consumption may potentiate the responsiveness of LH^{GAD2} neurons to CSs.

These findings highlight the potential role of LH^{GAD2} neurons in mediating consumption-induced regulation of learned freezing responses. Nevertheless, the precise neural circuit mechanisms underpinning this process require further investigation.

Synaptic connectivity of LH^{GAD2}-NI^{RLN3} circuit

To investigate the potential outputs of LH^{GAD2} neurons that mediate fear regulation through food consumption, we utilized engineered herpes simplex virus (HSV) to trace monosynaptic outputs from LH^{GAD2} neurons (Fig. 2a, “Methods” section). During this process, HSV-infected anterograde starter cells were identified in the LH (Fig. 2b). Following unilateral injection of helper virus and HSV into the LH, HSV-infected tdTomato-positive cells were detected in several ipsilateral brain regions with strong fluorescence intensity (Supplementary Fig. 5a). These regions included the nucleus of the horizontal limb of the diagonal band (HDB), ventral tegmental area (VTA), ventrolateral periaqueductal gray (vlPAG), and peri-locus coeruleus (periLC), which are known to receive projections from LH GABAergic neurons^{37–40}. We also observed a high number of HSV-infected cells in the NI. Given the role of the NI in stress responses^{28,29} and stressor-associated motivated ingestion behaviors^{30,31}, we investigated whether LH^{GAD2} neurons regulate fear during food consumption via projections to the NI. Following bilateral injection of helper virus and HSV into the LH, RNAscope in situ hybridization analysis revealed that a significant majority of LH^{GAD2}-innervating NI cells expressed *RLN3*. Moreover, most *RLN3*-positive NI neurons were transduced by HSV (Fig. 2c, d). These findings suggest that *RLN3* neurons are the primary downstream targets of LH^{GAD2} neurons within the NI, with most NI-resident *RLN3* neurons receiving direct projections from LH^{GAD2} neurons.

We conducted further analyses on LH cells projecting to NI^{RLN3} neurons using an engineered rabies virus (RV) (Fig. 2e, “Methods” section). RV-infected retrograde starter cells were identified in the NI (Fig. 2f). Notably, cells projecting to NI^{RLN3} neurons were found throughout the entire LH region, particularly in the middle to posterior regions (Supplementary Fig. 5b, c). RNAscope in situ hybridization revealed that most RV-infected LH cells ($74.84\% \pm 2.78\%$) expressed *GAD2*, with approximately one third of the cells ($35.28\% \pm 3.14\%$) co-expressing *GAD2* and *Slc17a6* (Fig. 2g, h). A significant number of these *GAD2*-positive LH cells ($65.34\% \pm 1.29\%$) also expressed *Slc32a1* (Supplementary Fig. 5d, e), while considerable proportion of RV-infected LH neurons ($28.45\% \pm 2.37\%$) co-expressed *Slc17a6* and *Slc32a1*

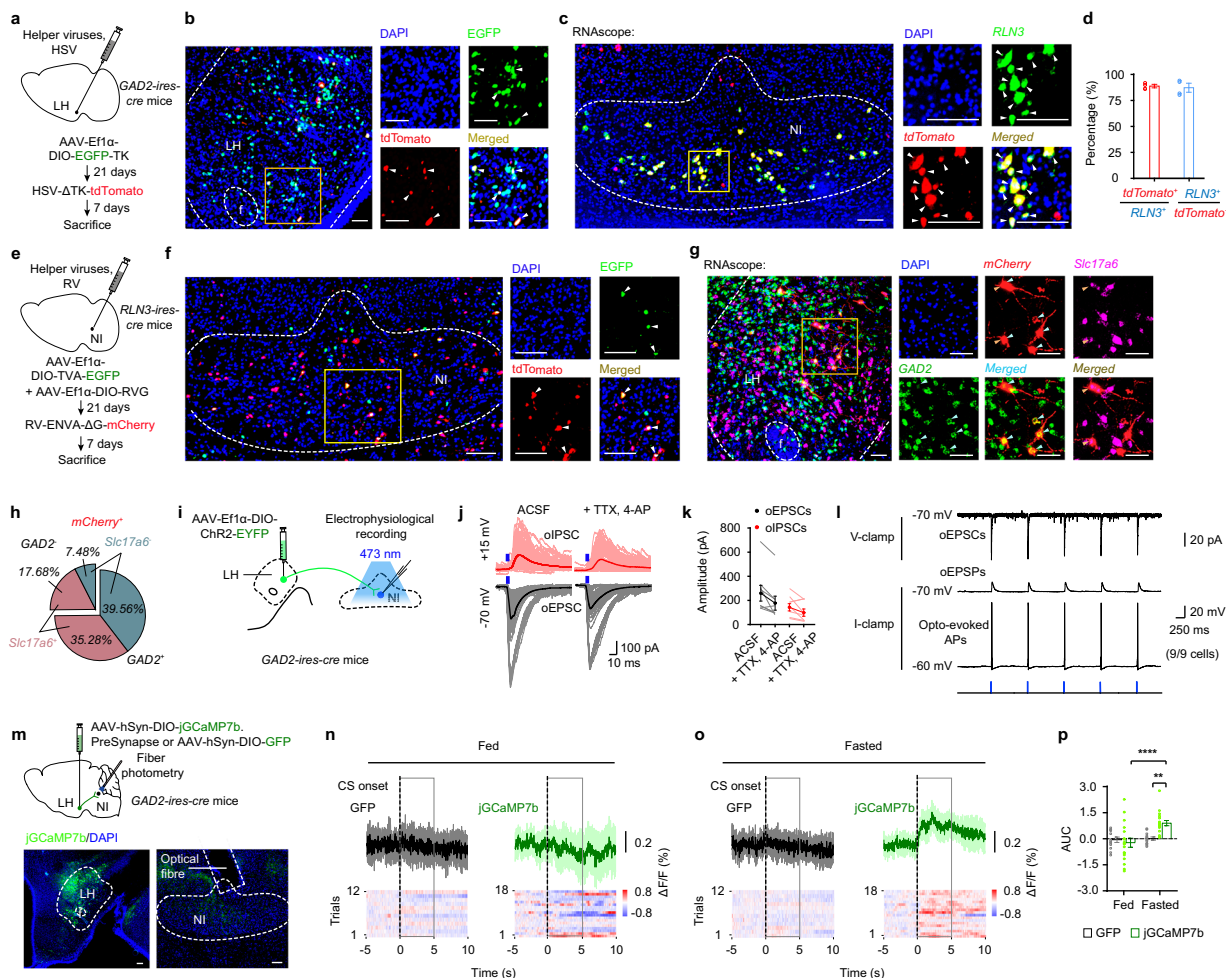


Fig. 2 | Synaptic connectivity of LH^{GAD2}-NI^{RLN3} circuit. **a** Anterograde tracing strategy of LH^{GAD2} neurons. **b** Representative fluorescence within the LH, with arrowheads indicating starter cells. **c** RNAscope in situ hybridization in the NI, with cells co-expressing *tdTomato* and *RLN3* denoted by arrowhead. **d** Percentage of cells co-expressing *tdTomato* and *RLN3*. *n* = 4 mice. **e** Retrograde tracing strategy of NI^{RLN3} neurons. **f** Representative fluorescence within the NI, with arrowheads indicating starter cells. **g** RNAscope in situ hybridization in the LH, with cyan arrowheads denoting *mCherry*-labeled *GAD2*-expressing cells which partially co-express *Slc17a6* as indicated by orange arrowheads. **h** Proportional distribution of RV-infected LH cells. *n* = 4 mice. **i** Schematic of electrophysiological recordings. **j** Traces of optogenetically evoked excitatory (oEPSCs) and inhibitory post-synaptic currents (oIPSCs) from NI neurons upon LH^{GAD2} fiber stimulation. TTX and 4-AP were dissolved in artificial cerebral spinal fluid (ACSF), with bath application. Gray and pink lines each represent 160 individual traces; dark and red lines each represent average; blue lines signify light stimulation. **k** Average oEPSC and oIPSC

amplitudes from photoactivated NI cells. *n* = 8 neurons/3 mice. **l** Representative traces of oEPSCs (above), opto-evoked excitatory post-synaptic potentials (oEPSPs; middle), and opto-evoked action potentials (APs; below) from photoactivated NI cells. *n* = 9 neurons/3 mice. **m** Schematic for LH^{GAD2}-NI GCaMP recordings (top) with representative image showing GCaMP transduction and implantation site of optical fiber (bottom). **n–p** LH^{GAD2}-NI fiber photometry signals in GFP- or jGCaMP7b-injected mice responding to conditioned stimulus (CS) under fed (**n**) and fasted (**o**) states. **n, o** Black dashed line indicates CS onset (time = 0); solid lines indicate average fluorescence traces, while shadings represent 95% confidence interval; gray frames show 5-s windows post-CS onset, which are used for calculations of area under the curve (AUC). **n–p** *n* = 12 trials/6 GFP mice, 18 trials/9 jGCaMP7b mice. Scale bar, 100 μ m. Data were presented as the mean \pm SEM; ***p* < 0.01, *****p* < 0.0001. Statistical significance was assessed using two-way repeated measures (RM) ANOVA with uncorrected Fisher's LSD multiple-comparisons test (**p**). Source data and exact *p* value are provided as a Source Data file.

(Supplementary Fig. 5f, g). Based on RNAscope in situ hybridization, the NI-projecting LH^{GAD2} neurons mainly included those neurons that expressed both *Slc32a1* and *Slc17a6* and those that expressed only *Slc32a1*. In addition, a small number of NI-projecting LH^{GAD2} neurons expressed only *Slc17a6* or neither (Supplementary Fig. 5h). There are two main theoretical possibilities for the projections of LH^{GAD2} neurons to the NI. One possibility is that the different types of LH^{GAD2} neurons project to the same NI neurons, forming both excitatory and inhibitory synaptic connections. The other possibility is that different types of LH^{GAD2} neurons project onto diverse NI neurons, each forming their own synaptic connections on different cells (Supplementary Fig. 5i). These results provide essential insights into the phenotypic characterization of the LH neurons involved. To detect the activity of these NI-projecting LH^{GAD2} neurons after the fear-feeding assay, we first used

a retrograde tracing strategy to label NI-projecting LH neurons (Supplementary Fig. 6a), then performed RNAscope in situ hybridization after the behavioral experiments. Results demonstrated a significant increase in the number of retrogradely labeled, *Fos*-expressing LH^{GAD2} neurons following CS exposure during food consumption in fasted fear-conditioned mice (Supplementary Fig. 6b, c).

To elucidate the synaptic functionality of the LH^{GAD2}-NI circuit, ex vivo electrophysiological recordings were combined with optogenetics (Fig. 2i, “Methods” section). Intriguingly, optogenetically evoked excitatory (oEPSCs) and inhibitory post-synaptic currents (oIPSCs) were recorded in identical NI cells. Of note, these signals persisted even in the presence of tetrodotoxin (TTX) and 4-aminopyridine (4-AP) (Fig. 2j, k), thereby indicating the existence of monosynaptic LH^{GAD2} inputs. Moreover, in optically responsive NI cells, stimulation of LH^{GAD2}

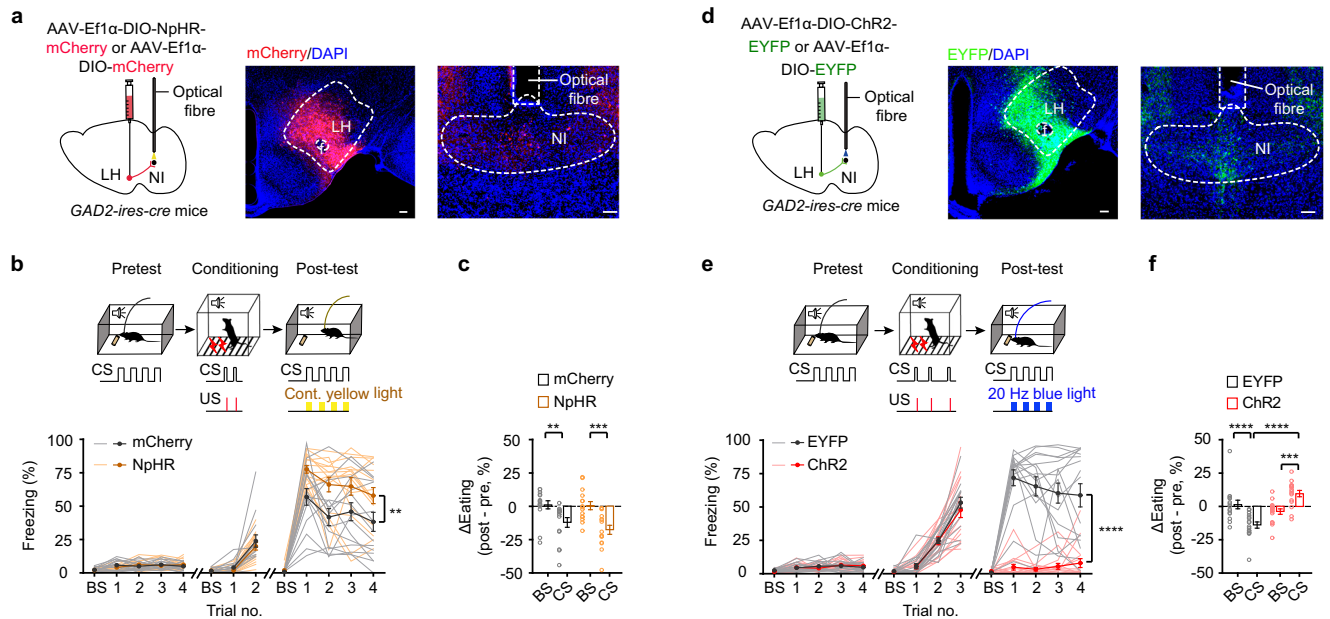


Fig. 3 | LH^{GAD2}-NI control of consumption-induced freezing regulation.

a Schematic for LH^{GAD2}-NI photoinhibition (left) with representative NpHR:mCherry distribution of transduced LH^{GAD2} somata (middle) and axons (right). Optical fiber was positioned above the NI. Scale bar, 100 μ m. **b** Photoinhibition of LH^{GAD2}-NI pathway increased freezing response in fear-conditioned mice during food consumption. Mice received two conditioned stimuli (CSs) paired with the unconditioned stimulus (US) during conditioning session. Continuous yellow light stimuli were applied during CSs of the post-test session (above), and freezing responses at baseline (BS) and during CSs were tested (down). Dark- and light-colored lines each represent average and individual, respectively. **c** Photoinhibition of LH^{GAD2}-NI terminals had no significant effect on fear-induced eating inhibition. The differences in eating time (Δ Eating) at BS and during CSs between the post-test and pretest sessions were assessed. **b**, **c** $n = 15$ mice/group. **d** Schematic of LH^{GAD2}-NI

photoactivation (left) with representative ChR2:EYFP distribution of transduced LH^{GAD2} somata (middle) and axons (right). Optical fiber was positioned above the NI. Scale bar, 100 μ m. **e** Photoactivation of LH^{GAD2}-NI pathway reduced freezing response of CS-conditioned mice during food consumption. Mice were subjected to three CSs paired with the US during conditioning session. 20 Hz blue light stimuli were applied during CSs of the post-test session (above), and freezing response to CS is shown (down). Dark- and light-colored lines each represent average and individual, respectively. **f** Photoactivation of LH^{GAD2}-NI pathway reversed fear-induced eating inhibition. **e**, **f** $n = 16$ mice/group. Data were presented as the mean \pm SEM; $**p < 0.01$, $***p < 0.001$, $****p < 0.0001$. Statistical significance was assessed using two-way RM ANOVA (**b**, **e**) or two-way repeated measures (RM) ANOVA with uncorrected Fisher's LSD multiple-comparisons test (**c**, **f**). Source data and exact p value are provided as a Source Data file.

fibers triggered either excitatory post-synaptic potentials (oEPSPs) or APs at membrane potentials of -70 mV and -60 mV, respectively (Fig. 2l). These findings suggest that the *Slc32a1*- and *Slc17a6*-positive LH^{GAD2} neurons likely form both excitatory and inhibitory synaptic connections on the same NI neurons, predominantly yielding excitatory outcomes. To detect the activity of the LH^{GAD2}-NI circuit during the fear-feeding assay, we recorded GCaMP signals from LH^{GAD2} terminals in the NI (Fig. 2m) as conditioned mice were exposed to CSs in both fed and fasted states, with unrestricted access to food. Results showed a significant increase in GCaMP activity in the LH^{GAD2}-NI terminals in response to CSs presented in the fasted state, but not in the fed state (Fig. 2n–p; Supplementary Fig. 6d, e). Conversely, no significant changes in LH^{GAD2}-NI GCaMP activity were observed when fasted mice began consuming food prior to or after CS presentation (Supplementary Fig. 6f–i). These results suggest that this circuit is specifically recruited during CS presentation in the context of food consumption, likely playing a role in regulating fear responses.

LH^{GAD2}-NI control of consumption-induced freezing regulation

The functionality of the LH^{GAD2}-NI circuit was further explored using optogenetic tools. We employed halorhodopsin (NpHR)-mediated circuit manipulation to inactivate the LH^{GAD2}-NI pathway (Fig. 3a; Supplementary Fig. 7a–d). Notably, inhibiting this circuit resulted in an aversive effect during real-time place preference (RTPP) tests (Supplementary Fig. 7e) and did not significantly impact normal food consumption in fasted mice (Supplementary Fig. 7f). Furthermore, LH^{GAD2}-NI inactivation disrupted the observed reduction in learned freezing response during food consumption (Fig. 3b), without significantly affecting CS-induced feeding inhibition (Fig. 3c). The

following day, when exposed to CSs in a different context while in a fed state, the CS-induced freezing responses were not influenced by LH^{GAD2}-NI photoinhibition (Supplementary Fig. 7g). These data suggest that the LH^{GAD2}-NI circuit modulates food consumption-induced regulation of learned freezing responses, without significantly affecting normal freezing responses in the fed state.

In contrast, we used the channelrhodopsin (ChR2)-mediated strategy to stimulate the LH^{GAD2}-NI circuit (Fig. 3d; Supplementary Fig. 7h–k). Activation of this circuit exerted a positive reinforcement effect on the RTPP test (Supplementary Fig. 7l) and enhanced normal food intake under both fed and fasted states (Supplementary Fig. 7m). Furthermore, stimulating the LH^{GAD2}-NI pathway resulted in reduced learned freezing responses during food consumption and reversed CS-induced inhibition of eating (Fig. 3e, f). The next day, in a different context and fed state, the ChR2-treated mice demonstrated slightly lower baseline freezing responses to CSs compared to the controls and LH^{GAD2}-NI photoactivation significantly decreased freezing responses (Supplementary Fig. 7n). To ensure that LH^{GAD2} neurons were not activated by the activity of their terminals in the NI, we activated LH^{GAD2}-NI terminals after TTX injection into the LH (Supplementary Fig. 8a). Results indicated that after LH silencing by TTX, photoactivation of the LH^{GAD2}-NI terminals still decreased learned freezing responses during food consumption (Supplementary Fig. 8b). TTX injection induced prolonged freezing responses in mice, possibly because the key role of the LH in arousal⁴¹ is suppressed by TTX. However, LH^{GAD2}-NI activation during CS still reduced the freezing response of fear-conditioned mice, while activation of the LH^{GAD2}-NI circuit after LH silencing did not reverse CS-induced inhibition of food consumption (Supplementary Fig. 8c). Thus, while this circuit can

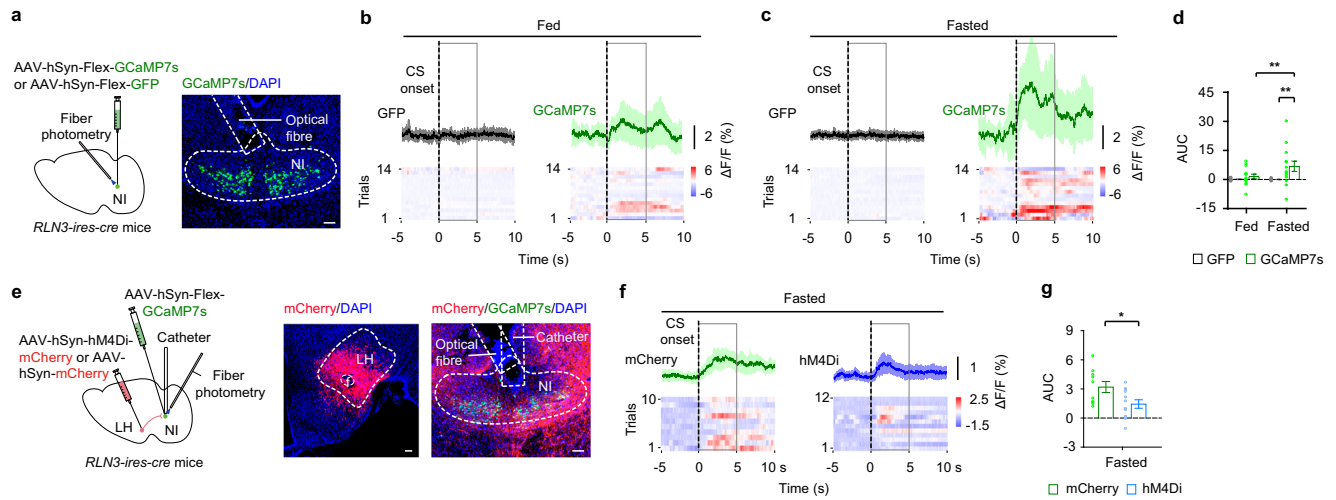


Fig. 4 | **NI^{RLN3} responses to CS presentation.** **a** Schematic for NI^{RLN3} GCaMP recordings (left) with representative image showing GCaMP transduction and implantation site of optical fiber (right). Scale bar, 100 μ m. **b–d** NI^{RLN3} fiber photometry signals in GFP- or GCaMP7s-injected mice responding to conditioned stimulus (CS) under fed (**b**) and fasted (**c**) states. The normalized change in fluorescence ($\Delta F/F$) was calculated. **b, c** Black dashed line indicates CS onset (time = 0); solid lines indicate average fluorescence traces, while shadings represent 95% confidence interval; gray frames show 5-s windows post-CS onset, which are used for calculations of area under the curve (AUC). **b–d** $n = 14$ trials/7 mice/group. **e** Schematic for NI^{RLN3} GCaMP recording accompanying inhibition of LH inputs (left), and representative image demonstrating GCaMP7s expression and

sites of optical fiber and cannula (right). Scale bar, 100 μ m. **f, g** NI^{RLN3} fiber photometry signals in fasted mCherry- or hM4Di-injected mice responding to CS after the infusion of clozapine-N-oxide (CNO) into the NI. **f** Black dashed line indicates CS onset (time = 0); solid lines indicate average fluorescence traces, while shadings represent 95% confidence interval; gray frames show 5-s windows post-CS onset, which are used for calculations of area under the curve (AUC). **f, g** $n = 10$ trials/5 mCherry mice, 12 trials/6 hM4Di mice. Data were presented as the mean \pm SEM; * $p < 0.05$, ** $p < 0.01$. Statistical significance was assessed using two-way repeated measures (RM) ANOVA with uncorrected Fisher's LSD multiple-comparisons test (**d**) or two-sided unpaired t -test (**g**). Source data and exact p value are provided as a Source Data file.

indeed reduce learned freezing responses, its effect on feeding may require the complete function of the LH, which is involved in feeding-related motivation, reward, and other functions⁴². Learned freezing responses were still reduced by the activation of this circuit in mice subjected to normal fear conditioning and post-test without food consumption (Supplementary Fig. 8d). Therefore, LH^{GAD2}-NI circuit activity can reduce learned freezing responses regardless of feeding. Overall, these findings provide evidence that LH^{GAD2}-NI circuit activity is both necessary and sufficient for food consumption regulation of learned freezing responses.

Given that nearly half of the LH^{GAD2} neurons projecting to the NI expressed *Slc17a6*, we investigated whether LH^{GAD2}-NI circuit function is mediated by general excitatory outputs from the LH to the NI. To explore this, we applied Chr2-mediated circuit activation of LH^{Vglut2}-NI pathway (Supplementary Fig. 9a). Activating this circuit induced an aversive effect on the RTPP test (Supplementary Fig. 9b) and triggered motion and jumping behaviors (Supplementary Fig. 9c–e), which markedly disrupted normal food consumption in fasted mice (Supplementary Fig. 9f). These effects are in stark contrast to those observed with LH^{GAD2}-NI activation. Thus, the excitatory outputs of the LH^{GAD2}-NI circuit represent only a subset of the projections from LH^{Vglut2} neurons to the NI, contributing specifically to the regulation of learned freezing responses during food consumption.

NI^{RLN3} responses to CS presentation

As LH^{GAD2}-NI outputs mainly innervated downstream RLN3 neurons, we next explored the role of NI^{RLN3} neurons in consumption-induced fear regulation. We first examined *Fos* gene expression in NI neurons after the fear-feeding assay. A substantial upregulation in *Fos* gene expression was observed in the NI^{RLN3} neurons of fasted-food mice relative to the fed-food group (Supplementary Fig. 10a–c).

Subsequently, GCaMP activity in NI^{RLN3} neurons was analyzed (Fig. 4a). In brief, mice subjected to fear conditioning were presented with CSs under both fed and fasted states, respectively, with

unrestricted access to food (Supplementary Fig. 10d). The results indicated that GCaMP activity in NI^{RLN3} neurons significantly increased in response to CSs when presented in the fasted but not fed state (Fig. 4b–d; Supplementary Fig. 10e, f). Conversely, NI^{RLN3} GCaMP activity in fasted mice significantly declined following eating onset prior to CS exposure. However, this decrease disappeared when conditioned mice recommenced eating post-CS presentation (Supplementary Fig. 10g–j). These findings suggest that NI^{RLN3} neurons specifically respond to CSs during food consumption, likely playing a critical role in learned freezing regulation, rather than directly influencing eating behavior.

To delineate the potential effects of LH inputs on NI^{RLN3} activity, we utilized a circuit-specific inhibitory strategy involving hM4Di-DREADD (designer receptors exclusively activated by designer drugs). Direct LH projections to the NI were inhibited while NI^{RLN3} GCaMP activity was recorded (Fig. 4e; Supplementary Fig. 11a). Injection of the DREADD ligand clozapine-N-oxide (CNO) into the NI 30 min prior to GCaMP recordings allowed for targeted suppression of the LH-NI pathway (Supplementary Fig. 11b). Notably, LH inputs led to a marked attenuation in the increase in NI^{RLN3} GCaMP responses to CSs during food consumption (Fig. 4f, g; Supplementary Fig. 11c, d). However, NI^{RLN3} activity associated with eating either before or after CS presentation remained unaffected by this intervention (Supplementary Fig. 11e–j).

Collectively, our results suggest a specialized role for NI^{RLN3} neurons in responding to CSs during food consumption, whereby CS-associated activities are controlled by LH inputs. Thus, these NI^{RLN3} neurons are likely instrumental in mediating food consumption-induced regulation of the learned freezing response.

NI^{RLN3} involvement in consumption-induced freezing regulation

To elucidate the functional role of NI^{RLN3} neurons in the regulation of the learned freezing response induced by food consumption, we employed NpHR-assisted optogenetic inhibition (Fig. 5a;

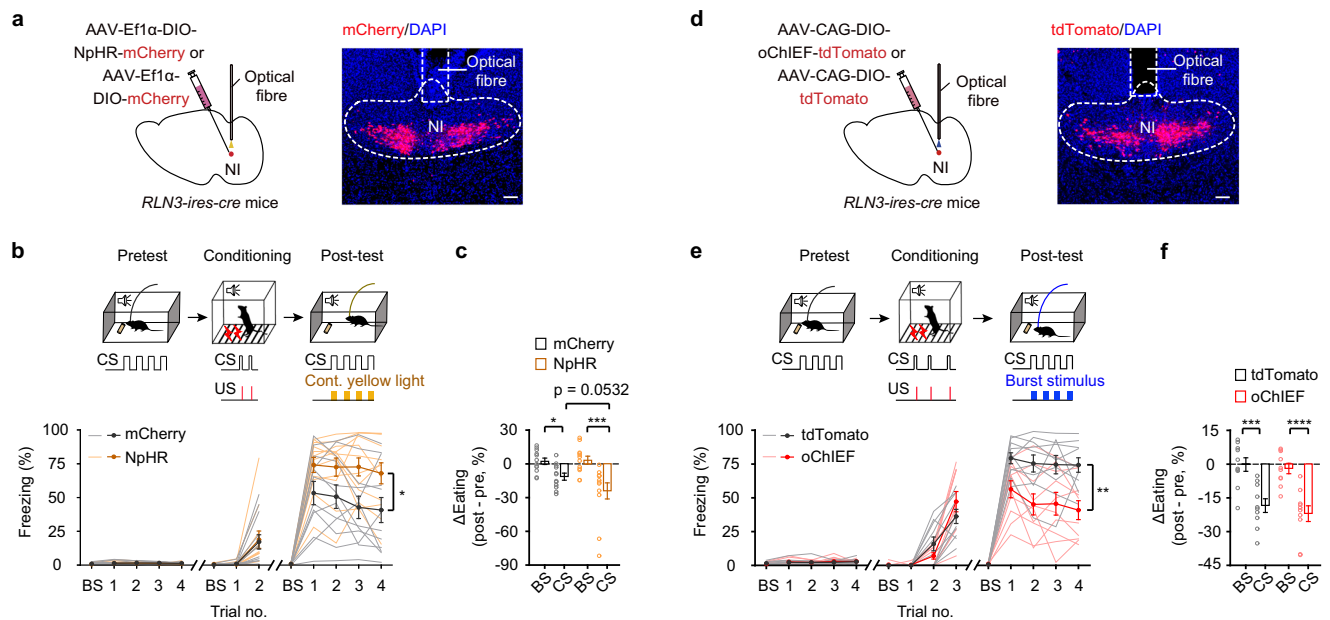


Fig. 5 | NI^{RLN3} involvement in consumption-induced freezing regulation.

a Schematic for NI^{RLN3} photoinhibition (left) with representative NpHR:mCherry distribution of transduced NI^{RLN3} somata (right). Optical fiber was situated above the NI. Scale bar, 100 μ m. **b** NI^{RLN3} photoinhibition increased freezing response of fear-conditioned mice during food consumption. Mice received two conditioned stimuli (CSs) paired with the unconditioned stimulus (US) during conditioning session. Continuous yellow light stimuli were applied during CS of the post-test session (above), and freezing responses at baseline (BS) and during CS were tested (down). Dark- and light-colored lines each represent average and individual, respectively. **c** NI^{RLN3} photoinhibition worsened fear-induced eating inhibition. The differences in eating time (Δ Eating) at BS and during CSs between the post-test and pretest sessions were assessed. **b, c** $n = 12$ mice/group. **d** Schematic for NI^{RLN3} photoactivation (left) with representative oChIEF:tdTomato distribution of

transduced NI^{RLN3} somata (right). Optical fiber was placed above the NI. Scale bar, 100 μ m. **e** NI^{RLN3} photoactivation led to a reduction in freezing response to CSs during food consumption. Mice received three CSs paired with the US during conditioning session. Burst stimulation of blue light was administered during CSs of the post-test session (above), and freezing responses at BS and during CS were tested (down). Dark- and light-colored lines each represent average and individual, respectively. **f** NI^{RLN3} photoactivation did not alter fear-induced eating inhibition. **e, f** $n = 10$ mice/group. Data were presented as the mean \pm SEM; * $p < 0.05$, *** $p < 0.001$, **** $p < 0.0001$. Statistical significance was assessed using two-way RM ANOVA (**b, e**) or two-way repeated measures (RM) ANOVA with uncorrected Fisher's LSD multiple-comparisons test (**c, f**). Source data and exact p value are provided as a Source Data file.

Supplementary Fig. 12a–d). This manipulation impaired the reduction in learned freezing response induced by food consumption (Fig. 5b) and slightly aggravated CS-induced suppression of eating (Fig. 5c). In addition, NI^{RLN3} inhibition demonstrated partial positive reinforcement in the RTPP test (Supplementary Fig. 12e), potentially attributable to a reduction in NI^{RLN3}-mediated behavioral activation and stress responses⁴³, and but had no observable effect on normal food consumption behaviors (Supplementary Fig. 12f).

Existing research suggests that neurons within the NI, particularly the RLN3-positive subset, exhibit burst-like firing patterns under in vivo conditions^{44–46}. To analyze firing patterns, we performed whole-cell recordings in EYFP-tagged NI^{RLN3} cells (Supplementary Fig. 13a). The average RMP for these neurons was approximately -57 mV (Supplementary Fig. 13b), with most cells displaying distinctive burst firing patterns in response to applied current injections (Supplementary Fig. 13c). Subjecting NI^{RLN3} neurons to ChR2-mediated 20-Hz light stimulation exerted no influence on food consumption-induced regulation of the learned freezing response (Supplementary Fig. 13d, e). Therefore, optogenetic burst stimulation using oChIEF, an opsin responsive to high-frequency light-pulse stimulation, was applied to activate the NI^{RLN3} neurons (Fig. 5d; Supplementary Fig. 13f–i). This stimulation generated a positive reinforcement effect on the RTPP test (Supplementary Fig. 13j) and diminished the learned freezing response during food consumption (Fig. 5e) but produced no effects on either CS-induced suppression of eating (Fig. 5f) or normal food consumption (Supplementary Fig. 13k).

Overall, these findings implicate NI^{RLN3} neurons as critical players in food consumption-induced regulation of learned freezing response, mediating LH^{GAD2}-NI circuit function.

NI^{RLN3}-LM output- and RLN3 signaling-mediated consumption regulation of freezing

To determine the functional downstream targets of NI^{RLN3} outputs, we first mapped these fibers to the whole brain, with dense EYFP fluorescent distributions observed in the accumbens shell (AcbSh), medial septum (MS), lateral preoptic area (LPO), LH, LM, and interpeduncular nucleus (IPN) (Supplementary Fig. 14a). After this, oChIEF-assisted circuit mapping was employed to confirm the functions of different NI^{RLN3} outputs (Supplementary Fig. 14b). Following fear conditioning, burst activation of NI^{RLN3} fibers in the LH and LM resulted in a decrease in the learned freezing response (Supplementary Fig. 14c, d). NI^{RLN3} projections to the LH may be involved in a feedback regulation mechanism integral to the LH^{GAD2}-NI circuit, while the LM may be a mediator of LH^{GAD2}-NI circuit function. We additionally determined the characteristics of LM neurons receiving NI^{RLN3} inputs by HSV anterograde tracing (Supplementary Fig. 14e). Anterograde starter cells infected by HSV were localized in the NI (Supplementary Fig. 14f). RNAscope in situ hybridization indicated that most HSV-infected LM neurons ($84.17\% \pm 1.73\%$) expressed the *Slc17a6* gene (Supplementary Fig. 14g, h; Supplementary Tables).

To determine the necessity of NI^{RLN3}-LM projections for the regulation of the learned freezing response induced by food consumption, we employed NpHR-assisted optogenetic inhibition to inactivate the NI^{RLN3}-LM pathway (Fig. 6a). This inactivation disrupted the observed reduction in the learned freezing response during food consumption (Fig. 6b), without significantly affecting CS-induced eating inhibition (Fig. 6c). These findings suggest that the NI^{RLN3}-LM circuit is involved in food consumption-induced regulation of learned freezing responses.

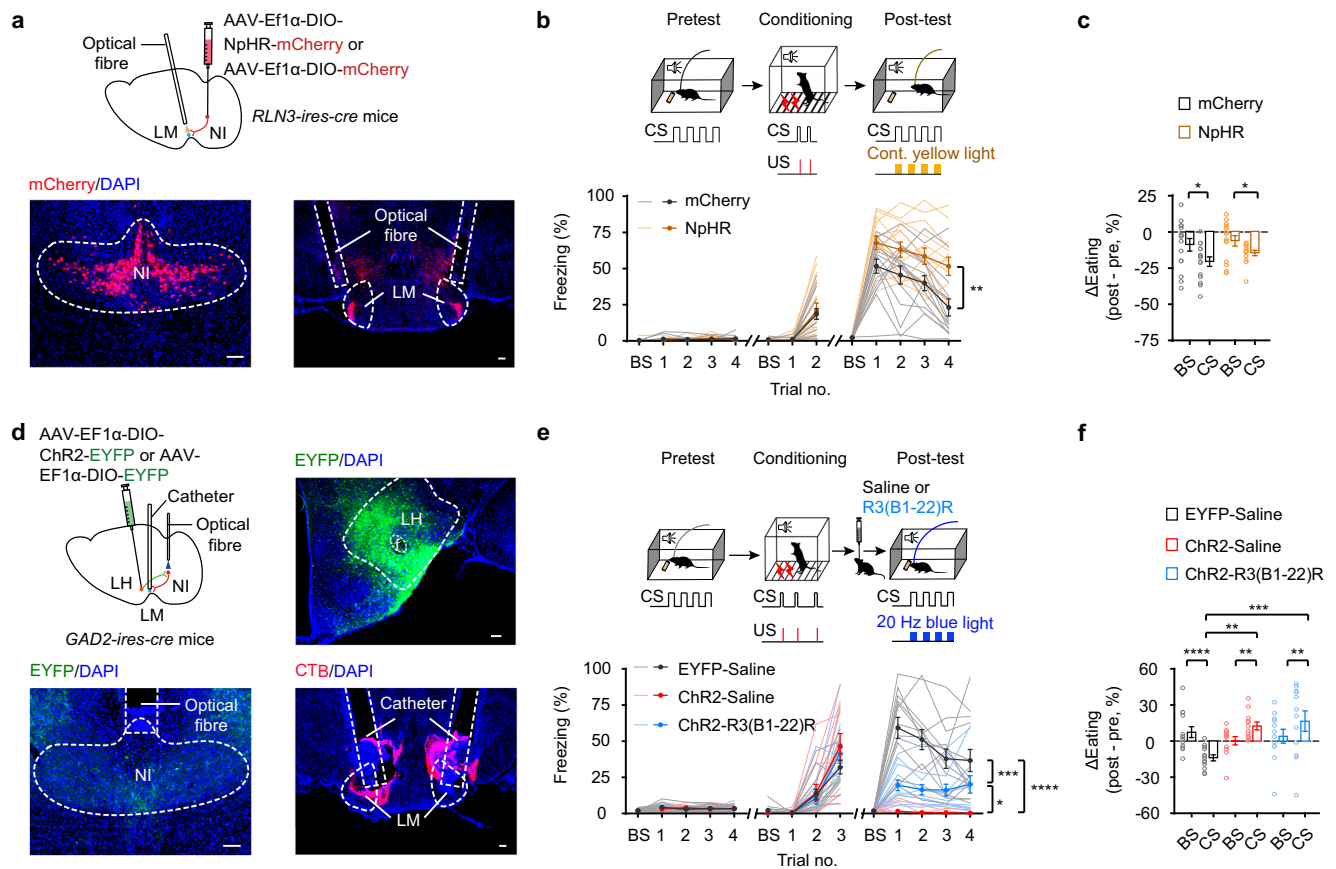


Fig. 6 | NI^{RLN3}-LM outputs- and RLN3 signaling-mediated consumption regulation of freezing. **a** Schematic for NI^{RLN3}-LM photoinhibition (top) with representative NpHR:mCherry distribution of transduced NI^{RLN3} somata and axons (bottom). Optical fiber was positioned above the LM. Scale bar, 100 μ m. **b** Photoinhibition of the NI^{RLN3}-LM pathway increased freezing response in fear-conditioned mice during food consumption. Mice received continuous yellow light stimulation during the conditioned stimulus (CS; above). Freezing responses at baseline (BS) and during CSs were tested (down). Dark- and light-colored lines each represent average and individual, respectively. **c** Photoinhibition of NI^{RLN3}-LM terminals had no significant effect on fear-induced eating inhibition. The differences in eating time (Δ Eating) at BS and during CSs between the post-test and pretest sessions were assessed. **b**, **c** $n = 15$ mCherry mice, 14 NpHR mice. **d** Schematic for LH^{GAD2}-NI photoactivation combined with LM blockade of RLN3 signaling (left), and representative ChR2:EYFP distribution of transduced LH^{GAD2} somata and axons (middle) and catheter position (right). Optical fiber was

placed above the NI. Catheter was implanted at an inclined angle at the top of the LM. Scale bar, 100 μ m. **e** LH^{GAD2}-NI photoactivation decreased freezing response of fear-conditioned mice during food consumption, with blockade of LM RLN3 signaling partly impairing this effect. Mice received relaxin-family peptide 3 receptor (RXFP3) antagonist or saline injection into the LM 15 min before behavioral experiments (above). Freezing responses at BS and during CSs were tested (down). Dark- and light-colored lines each represent average and individual, respectively. **f** LH^{GAD2}-NI photoactivation countered fear-induced eating inhibition insensitivity to LM blockade of RLN3 signaling. **e**, **f** $n = 13$ mice for EYFP-Saline group, 12 mice for ChR2-Saline, and ChR2-R3(B1-22)R group, respectively. Data were presented as the mean \pm SEM; * $p < 0.05$, ** $p < 0.001$, *** $p < 0.001$, **** $p < 0.0001$. Statistical significance was assessed using two-way RM ANOVA (**b**), two-way RM ANOVA with uncorrected Fisher's LSD multiple-comparisons test (**c**, **f**) or Tukey's multiple-comparisons tests (**e**). Source data and exact p value are provided as a Source Data file.

To verify the connection between LM-projecting NI^{RLN3} and LH^{GAD2} neurons, we used RV-mediated retrograde tracing (Supplementary Fig. 15a). Expression of both the helper virus and RV was detected in NI^{RLN3} neuronal bodies and terminals (Supplementary Fig. 15b, c). RNAscope in situ hybridization confirmed that a substantial number of RV-infected LH neurons ($42.53\% \pm 4.84\%$) expressed both the *GAD2* and *Slc17a6* genes (Supplementary Fig. 15d, e). These observations provide structural evidence supporting the existence of an LH^{GAD2}-NI^{RLN3}-LM circuit. RLN3 signaling, originating from the NI, is implicated in both eating- and anxiety-related behavior⁴⁷. Therefore, we assessed its function within the LH^{GAD2}-NI^{RLN3}-LM circuit via ChR2-assisted circuit activation in conjunction with relaxin-family peptide 3 receptor (RXFP3) inhibition (Fig. 6d; Supplementary Fig. 15f). Blockade of the RXFP3 receptors within the LM partially impaired the functionality of the LH^{GAD2}-NI circuit in regulating the learned freezing response during food consumption (Fig. 6e) but did not influence CS-induced suppression of eating (Fig. 6f).

Collectively, these findings suggest a critical role for both NI^{RLN3}-LM projections and associated RLN3 signaling in mediating the regulatory effects of the LH^{GAD2}-NI circuit in the learned freezing response induced by food consumption.

Discussion

Previous studies have predominantly focused on the impact of threats or stressors that induce negative emotions on feeding behaviors^{15,18–20,48,49}, as well as how appetitive behavior—particularly when driven by AgRP neurons in the Arc—interferes with fear or anxiety^{22–24}. In this research, we observed that food consumption regulated fear, specifically involving LH^{GAD2} neurons and their outputs to the NI. We further identified an LH^{GAD2}-NI^{RLN3}-LM circuit whose activity reduced learned freezing responses during food consumption.

Fear regulation by feeding is an active coping strategy

Here, we investigated how consuming regular chow, excluding the additional reward effects typically induced by high-fat and high-sugar

diets, regulates learned fear in male mice. This regulatory mechanism represents an adaptive processing of negative emotions driven by basic energy requirements.

Whether the decrease in learned freezing during food consumption is an active or passive behavior is unclear. In this study, fasted mice exposed to fear-CS during feeding exhibited mutually exclusive freezing responses or feeding behaviors. Thus, the observed decrease in freezing responses may be misconstrued as passive freezing regulation due to food consumption. We posit that fear regulation by feeding is an active behavior based on the following observations: first, when mice were subjected to CSs for the first time during feeding and LH^{GAD2}-NI activity increased, they remained in a freezing state, indicating activation of the antagonistic mechanisms of the brain despite the expression of fear behaviors. Second, when fasted mice were subjected to CSs during feeding, a 22.27% ± 5.10% decline in learned freezing responses was accompanied by a small 2.74% ± 1.63% increase in eating time during the fourth CS compared to the first CS, suggesting that the decrease in freezing was not caused by the direct antagonism of eating behavior. Therefore, it can be inferred that mice initially actively cope with fear before re-engaging in consummatory behaviors.

Active fear coping involves cortical arousal⁵⁰. The NI and its RLN3 signaling play a critical role in promoting arousal^{27,51–53}. Therefore, during feeding, mice may actively respond to potential dangers by increasing arousal, which may be an important mechanism of the LH^{GAD2}-NI circuit in regulating fear.

Freezing is an evolutionarily conserved passive fear response in rodents⁵⁴, with LH^{Vglut2} neurons likely playing an important role. Results showed that *Fos* gene expression in LH^{Vglut2} neurons increased in response to CSs, regardless of food consumption, consistent with research showing that LH^{Vglut2} neurons are involved in aversive behaviors⁷. In summary, we propose that mice subjected to aversive CSs during feeding primarily exhibit passive freezing responses and anorexia. However, a subset of GAD2 neurons in the LH is activated to antagonize this freezing response via the LH^{GAD2}-NI circuit, potentially facilitating a partial recovery of feeding behavior.

Possible mechanism of LH^{GAD2}-NI^{RLN3}-LM circuit for fear regulation

Fos gene analysis and GCaMP recordings demonstrated that LH^{GAD2} neurons were recruited to regulate fear responses during feeding. Electrophysiological data revealed an increase in the excitability of LH^{GAD2} neurons post-feeding, which may underlie their recruitment in response to fear-CSs during food consumption.

LH^{GAD2} neurons projected to RLN3 neurons in the NI, and activity within this circuit reduced the learned freezing response during feeding. These NI^{RLN3}-projecting LH^{GAD2} neurons included two main subpopulations, including those expressing both *Slc32a1* and *Slc17a6* and those expressing only *Slc32a1*. Interestingly, optogenetic activation of LH^{GAD2} terminals induced dual monosynaptic oEPSCs and oIPSCs on the same NI cell, ultimately forming an excitatory output. These findings imply that *Slc32a1*-positive and *Slc32a1/Slc17a6* double-positive LH^{GAD2} neurons likely form excitatory and inhibitory synaptic connections on the same NI cells. Upon LH^{GAD2}-NI axon stimulation, the oEPSCs peaked before the oIPSCs fully ascended, likely enhancing the signal-to-noise ratio of this circuit and facilitating information processing.

This study showed that the LH^{GAD2}-NI circuit regulated fear during feeding through the LM, although its precise functions remain unclear. The LM, located in the lateral part of the mammillary nucleus, is associated with head-direction perception^{55,56} and spatial learning^{57,58}. In the 5xFAD mouse model of Alzheimer's disease, LM neurons harbor aberrant hyperactivity, contributing to memory deficits⁵⁹. However, its role in regulating feeding and fear is not well understood. Given that RLN3 signaling frequently exhibits inhibitory effects in various brain

regions^{60–62}, we postulate that the inhibitory projection of NI^{RLN3} neurons to the mouse LM may reduce fear behavior by dulling perception of dangerous environments.

Multi-pathway mechanism by which LH GABAergic neurons relegate fear to promote feeding

In this study, activation of LH^{GAD2} terminals in the NI promoted food intake and reduced learned freezing responses, while activation of NI^{RLN3} neurons reduced learned freezing responses without affecting food intake. These results suggest that LH^{GAD2} projections to the NI, particularly to RLN3 neurons, primarily mediate the reduction of fear and freezing responses, while projections to other types of NI neurons or peripheral areas, such as the perILC³⁷, may mediate feeding behavior. As feeding behavior can antagonize freezing responses, the reduction in freezing caused by LH^{GAD2}-NI activation was more pronounced than that caused by direct activation of downstream NI^{RLN3} neurons, which may only suppress fear and freezing responses.

Given the potential role of the LH in coordinating feeding and aversive behaviors^{6–9}, we hypothesized that the synergistic action of LH outputs is required to alleviate fear-induced anorexia. When fear-conditioned mice received CSs during feeding, the dominant responses were CS-induced fear and anorexia, while a corresponding antagonistic mechanism was activated. In this process, LH^{GAD2} projections to NI^{RLN3} neurons predominantly reduce fear, while GABAergic outputs from the LH to other brain regions may promote feeding^{37–40}, partially alleviating fear-induced anorexia.

Based on our findings and existing studies, we propose the following model: when mice are energy deficient, AgRP neurons are activated⁶³, initiating appetitive behaviors^{22,64}. Once food is present and available, AgRP activity rapidly subsides^{65,66}, and putative LH neurons encoding food consumption become sequentially engaged¹², facilitating consummatory behaviors. When an animal encounters potential danger during food consumption, a subset of LH^{GAD2} neurons is actively recruited to adaptively regulate fear responses via the LH^{GAD2}-NI^{RLN3}-LM circuit. This regulation helps animals overcome fear responses and maintain minimum food consumption. Dysfunction in this regulation may be related to certain psychiatric disorders characterized by aberrant patterns of food consumption.

Limitations of the study

Further research is required to enhance our study. First, the mechanisms by which LH^{GAD2} neurons integrate signals that predict danger and promote feeding remain uncertain. Second, to gain a deeper understanding of the dynamics of the dual excitatory and inhibitory synapses of the LH^{GAD2}-NI circuit, the detailed structure of these synapses needs to be further investigated. Third, additional studies are necessary to elucidate how LM neurons receiving NI^{RLN3} outputs contribute to the reduction of learned freezing responses. Lastly, considering the intricate influence of estrogen and estrous cycles on fear behavior^{67,68}, feeding^{69,70}, and the relevant functions of the LH^{71,72} and NI⁷³, it is necessary to further investigate sex differences in the function of the LH^{GAD2}-NI^{RLN3}-LM circuit in mediating the regulation of fear by food consumption.

Methods

Mice

All experiments were conducted on male mice. To eliminate the potential variability introduced by estrogen and estrous cycles, we specifically excluded in female mice from the study. The mice were housed in a controlled environment under a 12-h light/dark cycle (light from 7 a.m. to 7 p.m.), with 4–5 mice/housing unit. In the raising and experimental room for mice, temperatures were maintained between 20 and 22 °C, and humidity levels ranged from 30% to 70%, with an average humidity of ~45%. The mice had free access to standard chow and sterile water, except for fasted mice. The experiments were

performed during daylight, with littermates randomly assigned across various experimental conditions. All mice were bred on a C57BL/6J background. Experimental procedures followed the National Institutes of Health Guidelines for the Care and Use of Laboratory Animals and were approved by the Animal Advisory Committee at Zhejiang University (ZJU2019-079). C57BL/6J mice were obtained from the Shanghai Laboratory Animal Center or The Jackson Laboratory (China). *GAD2-ires-Cre* (JAX Strain: 028867) and *Vglut2-ires-Cre* (JAX Strain: 028863) mice were originated from the Jackson Laboratory (USA), crossbred with the C57BL/6J lineage for over ten generations. The *RLN3-ires-Cre* mouse line was generated by Shanghai Model Organisms (China), with the C57BL/6J background. Mice aged 6–8 weeks were used for viral injection experiments, while 8–12-week-old mice were used for electrophysiological and behavioral studies.

Viruses

AAV2/9-Efl α -DIO-EGFP, AAV2/Retro-hsyn-Cre, AAV2/9-hSyn-Flex-GCaMP7s, AAV2/9-hSyn-Flex-GFP, AAV2/9-Efl α -DIO-hChr2(H134R)-EYFP, AAV2/9-Efl α -DIO-eNpHR3.0-mCherry, AAV2/9-Efl α -DIO-EYFP, AAV2/9-Efl α -DIO-mCherry, AAV2/9-hSyn-hM4D(Gi)-mCherry, and AAV2/9-hSyn-mCherry were purchased from OBIO Technology (China). AAV2/9-hsyn-DIO-jGCaMP7b.PreSynapse was purchased from Shanghai Taitool Bioscience (China). AAV2/8-Efl α -DIO-EGFP-T2A-TK, HSV- Δ TK-tdTomato, AAV2/9-Efl α -DIO-EGFP-T2A-TVA, AAV2/9-Efl α -DIO-RVG, and RV-EvnA- Δ G-mCherry were purchased from BrainVTA (China). AAV2/9-CAG-DIO-oChIEF (E163A/T199C)-tdTomato and AAV2/9-CAG-DIO-tdTomato were obtained from Brain Case (China).

All viruses, with titers $>1.0 \times 10^{12}$ genome copies/mL, were aliquoted and stored at -80°C until use. A minimum waiting period of 4 weeks post-injection was observed to ensure sufficient viral expression.

Virus injection and stereotaxic surgery

Mice were anesthetized with 0.5% pentobarbital sodium (0.015 mL/g, Trinnity Drug Store, USA) and placed in a stereotaxic frame (RWD Life Science, China) for small craniotomies. A pulled-glass pipette (tip diameter, 20–50 μm), attached to a microinjector pump (RWD Life Science), was used for viral microinjection at the following brain coordinates (referring to bregma; anteroposterior, AP; mediolateral, ML; dorsoventral, DV; in mm): LH: AP -1.70 , ML ± 0.95 , DV -5.25 ; NI: AP -5.00 , ML ± 0.00 , DV -4.25 ; and LM: AP -2.20 , ML ± 1.65 , DV -5.10 , with a 10° angle.

For in vivo fiber photometry, optical fibers (diameter, 200 μm ; numerical aperture, 0.37; Inper, China) were implanted unilaterally at the following coordinates (in mm): LH: AP -1.70 , ML $+0.95$, DV -5.15 ; NI: AP -4.90 , ML $+2.00$, DV -3.60 , angled 30° horizontally from the anterior to posterior side and 30° vertically from the midline to lateral side. For in vivo optogenetics, the same optical fibers were implanted at the following coordinates (in mm): NI: AP -5.20 , ML ± 0.00 , DV -4.00 ; LM: AP -2.20 , ML ± 1.65 , DV -4.85 (10° angle); vNacSh: AP $+2.45$, ML ± 1.60 , DV -4.80 (10° angle); MS: AP $+1.60$, ML $+0.75$, DV -3.50 (10° angle); LPO: AP $+0.45$, ML ± 2.15 , DV -4.80 (10° angle); IPN: AP -2.70 , ML ± 0.95 , DV -4.05 (10° angle); LH: AP -1.00 , ML ± 1.00 , DV -5.10 .

For intra-brain drug infusion, guide cannulas (26 G, 3.30-mm length, RWD Life Science) were implanted at the following coordinates (in mm): NI: AP -5.20 , ML ± 0.00 , DV -3.30 ; LM: AP -2.20 , ML ± 1.65 , DV -4.20 , with an angle of 10° . Obturators were inserted into the guide cannulas until the experiments. Injection cannulas (33 G, 3.30 mm + 1.0 mm projection, RWD Life Science) were inserted into the guide cannulas and connected to a microinfusion pump (RWD Life Science) for drug infusion. Clozapine-N-oxide (CNO, 1 mM, 300 nl; Sigma-Aldrich, USA, SML2304) or RXFP3 inhibitor (B3(B1-22)R, 400 ng/side; Phoenix Pharmaceuticals, USA, 035-36A) was infused over 2 min, with another 2 min for solution diffusion. Mice then returned to their home cages and rested for 30 min until behavioral testing.

After the experiments, the accuracies of the viral injection and optical fiber and cannula implantation sites were verified by fluorescent protein and residual tracks.

For labeling LH^{GAD2} neurons in ex vivo electrophysiological recordings, Cre-dependent EYFP-expressing AAV vector (AAV-DIO-EYFP) were bilaterally injected into the LH of *GAD2-ires-Cre* mice at least 2 weeks prior to the experiment. Similarly, to label NI^{RLN3} neurons, AAV-DIO-tdTomato were injected into the NI of *RLN3-ires-Cre* mice.

HSV- and RV-based monosynaptic tracing

For anterograde monosynaptic tracing, AAV-Efl α -DIO-EGFP-T2A-TK was injected to Cre-dependently express thymidine kinase (TK). At 21 days after the first injection, genetically modified HSV (HSV- Δ TK-tdTomato) with TK deficiency was injected. Putative starter cells of HSV tracing were co-expressing tdTomato and EGFP. For retrograde transsynaptic tracing, a mixture of two helper viruses Cre-dependently expressing avian tumor virus receptor A (AAV-Efl α -DIO-EGFP-T2A-TVA) and RV glycoprotein (AAV-Efl α -DIO-RVG), respectively (1:1 volume ratio), were first injected. After 21 days, EnvA-pseudotyped, glycoprotein (RG)-deleted, and mCherry-expressing RV (RV-EvnA- Δ G-mCherry) were injected. An additional 7 days were allocated for HSV/RV expression. Putative starter cells of RV tracing were co-expressing mCherry and EGFP.

RNAscope in situ hybridization

Coronal sections (20- μm thickness) were first prepared as per standard protocols. Briefly, mice were deeply anesthetized with isoflurane (RWD Life Science), then transcardially perfused with 30 mL of 0.9% saline solution, followed by 30 mL of 4% paraformaldehyde (PFA, Sigma-Aldrich, 158127) in phosphate-buffered saline (PBS). Their brains were then removed and fixed in 4% PFA for 24 h, followed by cryoprotection in a 30% sucrose solution buffered with PBS for at least 72 h at 4°C . Coronal sections of the preserved brains were prepared using a freezing microtome (Leica), each to a thickness of 20 μm . Subsequently, the sections were mounted on glass slide for desiccation and storage at -80°C . The RNAscope Multiplex Fluorescent v2 Assay in conjunction with corresponding mouse-origin probes (ACDbio, USA) was then used to measure the expression of the following genes (Probe Catalog No.): *GAD2* (439371), *Slc32a1* (319191), *Slc17a6* (319171), *RLN3* (459921), *tdTomato* (317041), *Fos* (439371), and *mCherry* (31201). All experiments were carried out according to the manufacturer's guidelines (see Supplementary Methods for detailed information).

Slice whole-cell recording

Slices for electrophysiological recording were prepared as per our previous study⁷⁴. Briefly, mice first underwent deep anesthesia with isoflurane (RWD Life Science), and transcardial perfusion of the ice-cold sucrose-based artificial cerebrospinal fluid (ACSF, in mM): 230 sucrose, 2.5 KCl, 10 MgSO₄, 0.5 CaCl₂, 1.25 NaH₂PO₄, 26 NaHCO₃, 10 glucose and 1.5 pyruvate, saturated with 95% O₂ and 5% CO₂. After decapitation, brains were transferred quickly into ice-cold sucrose-based ACSF bubbled with 95% O₂ and 5% CO₂, and coronal brain sections with a thickness of 300 μm were then prepared using a Leica VT1000S Vibratome (Leica, VT1200, Germany), followed by incubation for 1–4 h at room temperature prior to recording. The ACSF for recording contained (in mM): 126 NaCl, 2.5 KCl, 1.25 NaH₂PO₄, 26 NaHCO₃, 2 CaCl₂, 2 MgCl₂, and 10 glucose, saturated with 95% O₂ and 5% CO₂. Whole-cell patch-clamp recordings were executed at room temperature, with the aid of a MultiClamp 700B amplifier (low-pass 2-kHz filtering, digitization at 10 kHz; Molecular Devices, USA) in conjunction with a 1440A interface (Molecular Devices) and pClamp software v10.4 (Molecular Devices). Illumination for visualizing fluorescent cells was provided by 473-nm blue light or 589-nm yellow light delivered via an LED source (Polygon400, Mightex, USA). To detect membrane potentials, the recording electrodes were filled with a

potassium gluconate-based internal solution including (in mM): 140 K-gluconate, 5 KCl, 10 HEPES, 0.2 EMBA, 2 MgCl₂, 4 Mg-ATP, 0.3 Na₂-GTP, and 10 Na₂-phosphocreatine, calibrated to pH 7.2, with resistances between 4 and 5 MΩ. To record post-synaptic currents, recording electrodes with resistances between 3 and 4 MΩ were filled with a Cs-methanesulfonate-based internal solution comprising (in mM): 115 Cs-methanesulfonate, 20 CsCl, 10 HEPES, 2.5 MgCl₂, 4 Na₂-ATP, and 10 Na₂-phosphocreatine, adjusted to pH 7.2. All drugs for the preparation of ACSF and internal solution were purchased from Sigma-Aldrich.

Under current-clamp mode, the stable resting membrane potential (RMP) was measured and averaged over a 60-s duration with 0-mA current injection immediately after establishing whole-cell recordings. Input resistance (R_{in}) was determined by injecting a -100-pA current into the neuron and dividing the hyperpolarization-induced voltage change by the injected current. To quantify the firing rates of recorded neurons, membrane potentials were first maintained at a baseline level of -70 mV, and the number of action potentials (APs) fired in response to a 200-ms pulse of depolarizing current injection was assessed. For LH^{GAD2} neurons, the current threshold was defined as the minimal current injection (5-pA increments) that could trigger the first APs. For NI^{RLN3} neurons, each burst was defined as a series containing at least three APs, each separated by an inter-AP interval shorter than 100 ms, with burst intervals extending beyond 200 ms.

To examine LH^{GAD2}-NI synaptic properties, 5-ms light pulses (-1.6 mW mm⁻²) at 1 Hz were delivered to optogenetically evoke post-synaptic currents. Voltage-clamp recordings were used to isolate oEPSCs and oIPSCs by holding potentials (V_h) at -70 and +15 mV, respectively. Light stimulation lasted for 10 s, repeated twice. To inhibit multisynaptic responses, ACSF enriched with both tetrodotoxin (TTX, 1 mM; Tocris Bioscience, UK, 4368-28-9) and 4-aminopyridine (4-AP, 100 mM; Sigma-Aldrich, 275875) was perfused into slices for a minimum of 10 min. The oEPSCs and oIPSCs were again recorded using the same protocols as above. To assess the excitability of post-synaptic neurons in response to optogenetic activation of LH^{GAD2} fibers, optically responsive NI cells were first identified through oEPSC recordings. Subsequently, under current-clamp configuration, these cells received 5-ms light pulses (-1.6 mW mm⁻², 1 Hz, 5 s).

To establish the validity of opsin viruses, current-clamp recordings were implemented to assess the excitability of infected cells in response to optical stimulation. The EYFP or mCherry-labeled ChR2 or NpHR-infected cells were patched and received 5-ms 473-nm light pulses (-1.6 mW mm⁻², 20 Hz, 5 s) or continuous 589-nm light (-2.0 mW mm⁻², 5 s). The tdTomato-labeled, oChIEF-infected NI cells were patched and received burst stimuli of 5-ms 473-nm light pulses (-1.6 mW mm⁻², 30 Hz) for 15 pulses, each lasting 200 ms, separated by an inter-burst interval of 100 ms. All collected data were measured and analyzed using Clampfit v10.7 software (Molecular Devices).

Behavioral tasks

In both ChR2/oChIEF-mediated optostimulation and NpHR-mediated optoinhibition experiments, optical fibers were connected to 473-nm and 563-nm laser devices (Inper), respectively. The laser power was regulated between 4–6 mW for ChR2/oChIEF and 10–12 mW for NpHR in each experiment.

Fear-feeding assay

Pavlovian fear conditioning was integrated with feeding behavior to investigate learned freezing responses during food consumption, called the fear-feeding assay. In brief, the mice first underwent three feeding training sessions, during which they were fasted for 24 h, then given unrestricted access to chow in the feeding chamber. Each session lasted 10 min, with the addition of four sounds from a buzzer (76 dB, lasting 1 min each) separated at 1-min intervals. In the subsequent pretest and post-test sessions, the mice were fasted for 24 h and likewise received the sounds four times in 10 min, with free food

consumption. Between the two sessions, mice were successively subjected to fear conditioning and another 10-min feeding training session devoid of CS. During the fear conditioning session, mice received sounds (76 dB, lasting 30 s each) two or three times as a CS, paired with co-terminating foot shocks as an unconditioned stimulus (US; 0.5 mA, 2 s each), at variable intervals (60–160 s). Each session of the fear-feeding assay was scheduled on different days, and fasting for 2 consecutive days was avoided. The behaviors of mice in the pretest, conditioning, and post-test sessions were video-recorded, and freezing and eating times during baseline and CS were analyzed. In the post-test session, changes in food consumption (Δ Eating (%)) during CS or at baseline (BS) were normalized by calculating the percentage difference between the eating time during CS or BS in the post-test session and the same period in the pretest session.

To investigate how fear is regulated by food consumption in naïve C57 mice (Fig. 1a–d), we categorized conditioned mice into three groups in the post-test session: fed-food, fast-no food, and fast-food. During the conditioning session, all three groups of mice received two CSs paired with the US. However, in the post-test session, the conditions differed among the three groups: fed-food mice were satiated and given unrestricted access to food, fast-no food mice were fasted for 24 h and not provided with food, and fast-food mice were fasted for 24 h and allowed to freely consume food. These mice were sacrificed 30 min after the post-test session to conduct *Fos* gene analysis on LH and NI neurons following the fear-feeding assay.

For ex vivo electrophysiological recordings of LH^{GAD2} neurons after the fear-feeding assay, EYFP-labeled *GAD2-ires-Cre* mice were divided into four groups: home cage, fed-food, eating-only, and fast-food. During the conditioning session, all four groups of mice received two CSs paired with the US. Two hours before the electrophysiological experiments, mice in the fed-food and fasted-food groups were placed in feeding chambers for 20 min under fed and fasted conditions, accordingly, with unrestricted access to food. During this period, the mice received CSs four times in the first 10 min. Mice in the eating-only group were fasted and allowed to freely eat food for 20 min. As a control, mice in the home cage group were housed in their home cages with uninhibited access to food until the initiation of electrophysiological recordings.

For the in vivo optogenetic experiments of the fear-feeding assay, a light stimulus was delivered during CS in the post-test sessions of fasted mice. The day after the post-test sessions, mice in a fed state were presented with CSs four times. Light stimulus was then delivered concurrently with the final two CS presentations.

In vivo fiber photometry and data analysis

GCaMP fluorescence intensities were recorded using fiber photometry and analyzed as described in previous studies^{74,75}. Briefly, GCaMP signals were obtained using a multi-channel fiber photometry device (Inper) in conjunction with Inper Studio software (Inper), in which two light sources (470 and 410 nm) were administered alternately, with 410 nm serving as the internal control. A 410-nm non-GCaMP-sensitive excitation light was used to obtain background fluorescence signals, which served to correct the GCaMP signal obtained with 470-nm excitation light⁶⁸. The corrected GCaMP signal was used for further analysis. The normalized change in fluorescence ($\Delta F/F$) was calculated by subtracting baseline fluorescence from fiber fluorescence at each time point, then dividing the result by baseline fluorescence. Processing and analysis of photometric data were conducted using the Inper Data Process (v0.5.9, Inper) tool. Similar to the fear-feeding assay described above, mice first underwent feeding training, pretesting, fear conditioning, and post-conditioning feeding training sequentially. The conditioned mice were then exposed to two CSs (60 s each) in the presence of chow under a fed state or after 24 h of fasting, respectively, with GCaMP signals continuously recorded for 10 min. GCaMP responses to the CSs, as well as eating onset before and after CS

presentation, were analyzed, with a 5- or 10-s baseline taken before time 0, corresponding to CS and eating onset, respectively. The area under the curve (AUC) for the $\Delta F/F$ curves within another 5- or 10-s window after time 0 was calculated using the trapezoidal method in GraphPad Prism (v10.0.0(153), GraphPad Software, USA).

For in vivo NI^{RLN3} fiber photometry combined with chemogenetic inhibition of LH inputs, CNO was infused into the NI 30 min prior to the experiment. Conditioned mice fasted for 24 h were exposed to two CSs during food consumption, with concurrent recording of GCaMP signals for 10 min.

Real-time place preference (RTPP) test

Mice were placed in a home-made Plexiglas box with two interconnected chambers, each measuring $50 \times 50 \times 50$ cm, for 20 min of free exploration. Time spent in each chamber was measured to establish baseline preference, with one of the chambers designated as the stimulation side. On the 2nd day, the mice were initially placed in the non-stimulation side to begin the experiment. Once they moved to the stimulation side, the mice received light stimulation, which stopped when they re-entered the non-stimulation side. Time spent in both chambers was again measured for 20 min. Mouse behaviors were recorded using a CCD camera paired with ANY-maze software (v.7.2.0; Stoelting Company, USA). This software facilitated control over laser stimulation and extraction of various behavioral parameters. The preference changes for the stimulation chamber between baseline and testing were evaluated.

Free food consumption test

Mice were fasted for 24 h and allowed to freely eat chow. This training lasted for 20 min and was conducted twice to habituate the mice to the experimental operation. On the day of the experiment, the mice were either fed or fasted for 24 h beforehand. In the experiment, mice had free access to chow for two 20-min phases, with only the second phase paired with light stimulus. Food consumed in each phase was recorded, and the differences between the two were analyzed.

Open field test

Mice were first placed into the central zone of an open field chamber, measuring $42 \times 42 \times 42$ cm. They were tethered to the optical-fiber patch cords and allowed to freely explore for 15 min, divided into three 5-min phases, with only the second phase paired with light stimulus. The paths mice took were recorded using a video camera and analyzed using Any-maze software. Locomotor distances and jumping number were evaluated for each 5-min phase.

Statistical analysis

All experiments and data analyses were conducted in a double-blind manner. The number of replicates (n) indicated in the figure legends corresponds to the number of experimental subjects independently treated under each experimental condition. Animals with misplaced viral injection or incorrect fiber and cannula placement were excluded from analysis. Data are represented as either mean \pm standard error of the mean (SEM) or 95% confidence interval (CI), as noted in the figure legends. All statistical values for average cell count and percentage in RNAScope in situ hybridization were provided in Supplementary Table. For statistical comparisons, GraphPad Prism was used along with appropriate inferential methods, as specified in the figure legends. Normally distributed data were analyzed using one- or two-way analysis of variance (ANOVA), followed by appropriate multiple-comparisons test proposed by GraphPad Prism software. Student's t -tests were utilized for comparisons between two groups unless specifically noted otherwise. Neither sample size predetermination nor statistical randomization methods were employed in this study. All tests were two-tailed. A significance level of 0.05 was used for all hypothesis testing.

Reporting summary

Further information on research design is available in the Nature Portfolio Reporting Summary linked to this article.

Data availability

All supporting data generated in this study are provided in the Supplementary Information and Source Data files. Source data are provided with this paper and are also available in the Figshare database at <https://doi.org/10.6084/m9.figshare.24717987>.

References

1. Stunkard, A. J., Faith, M. S. & Allison, K. C. Depression and obesity. *Biol. Psychiatry* **54**, 330–337 (2003).
2. Simon, G. E. et al. Association between obesity and psychiatric disorders in the US adult population. *Arch. Gen. Psychiatry* **63**, 824–830 (2006).
3. Johnston, E., Johnson, S., McLeod, P. & Johnston, M. The relation of body mass index to depressive symptoms. *Can. J. Public Health* **95**, 179–183 (2004).
4. Thomas, M. A. & Xue, B. Mechanisms for AgRP neuron-mediated regulation of appetitive behaviors in rodents. *Physiol. Behav.* **190**, 34–42 (2018).
5. Gouveia, A., de Oliveira Belez, R. & Steculorum, S. M. AgRP neuronal activity across feeding-related behaviours. *Eur. J. Neurosci.* **54**, 7458–7475 (2021).
6. Rossi, M. A. et al. Transcriptional and functional divergence in lateral hypothalamic glutamate neurons projecting to the lateral habenula and ventral tegmental area. *Neuron* **109**, 3823–3837.e3826 (2021).
7. Jennings, J. H., Rizzi, G., Stamatakis, A. M., Ung, R. L. & Stuber, G. D. The inhibitory circuit architecture of the lateral hypothalamus orchestrates feeding. *Science* **341**, 1517–1521 (2013).
8. Stuber, G. D. & Wise, R. A. Lateral hypothalamic circuits for feeding and reward. *Nat. Neurosci.* **19**, 198–205 (2016).
9. Rossi, M. A. & Stuber, G. D. Overlapping brain circuits for homeostatic and hedonic feeding. *Cell Metab.* **27**, 42–56 (2018).
10. Berthoud, H. R. & Munzberg, H. The lateral hypothalamus as integrator of metabolic and environmental needs: from electrical self-stimulation to opto-genetics. *Physiol. Behav.* **104**, 29–39 (2011).
11. Lee, Y. H. et al. Lateral hypothalamic leptin receptor neurons drive hunger-gated food-seeking and consummatory behaviours in male mice. *Nat. Commun.* **14**, 1486 (2023).
12. Jennings, J. H. et al. Visualizing hypothalamic network dynamics for appetitive and consummatory behaviors. *Cell* **160**, 516–527 (2015).
13. Sharpe, M. J. et al. Lateral hypothalamic GABAergic neurons encode reward predictions that are relayed to the ventral tegmental area to regulate learning. *Curr. Biol.* **27**, 2089–2100.e2085 (2017).
14. Barbano, M. F., Wang, H. L., Morales, M. & Wise, R. A. Feeding and reward are differentially induced by activating GABAergic lateral hypothalamic projections to VTA. *J. Neurosci.* **36**, 2975–2985 (2016).
15. Petrovich, G. D., Ross, C. A., Mody, P., Holland, P. C. & Gallagher, M. Central, but not basolateral, amygdala is critical for control of feeding by aversive learned cues. *J. Neurosci.* **29**, 15205–15212 (2009).
16. Ohata, H. & Shibasaki, T. Involvement of CRF2 receptor in the brain regions in restraint-induced anorexia. *Neuroreport* **22**, 494–498 (2011).
17. Qu, N. et al. A POMC-originated circuit regulates stress-induced hypophagia, depression, and anhedonia. *Mol. Psychiatry* **25**, 1006–1021 (2019).
18. Xu, Y. et al. Identification of a neurocircuit underlying regulation of feeding by stress-related emotional responses. *Nat. Commun.* **10**, 3446 (2019).
19. Nagashima, T. et al. Parabrachial-to-parasubthalamic nucleus pathway mediates fear-induced suppression of feeding in male mice. *Nat. Commun.* **13**, 7913 (2022).

20. Yang, B. et al. Locus coeruleus anchors a trisynaptic circuit controlling fear-induced suppression of feeding. *Neuron* **109**, 823–838.e826 (2021).
21. Salgado, I. D. et al. Toggling between food-seeking and self-preservation behaviors via hypothalamic response networks. *Neuron* **111**, 2899 (2023).
22. Padilla, S. L. et al. Agouti-related peptide neural circuits mediate adaptive behaviors in the starved state. *Nat. Neurosci.* **19**, 734–741 (2016).
23. Burnett, C. J. et al. Hunger-driven motivational state competition. *Neuron* **92**, 187–201 (2016).
24. Dietrich, M. O., Zimmer, M. R., Bober, J. & Horvath, T. L. Hypothalamic AgRP neurons drive stereotypic behaviors beyond feeding. *Cell* **160**, 1222–1232 (2015).
25. Petzold, A., van den Munkhof, H. E., Figge-Schlensock, R. & Kortkova, T. Complementary lateral hypothalamic populations resist hunger pressure to balance nutritional and social needs. *Cell Metab.* **35**, 456 (2023).
26. Gong, R., Xu, S., Hermundstad, A., Yu, Y. & Sternson, S. M. Hindbrain double-negative feedback mediates palatability-guided food and water consumption. *Cell* **182**, 1589–1605.e1522 (2020).
27. Ma, S. et al. Nucleus incertus promotes cortical desynchronization and behavioral arousal. *Brain Struct. Funct.* **222**, 515–537 (2017).
28. Tanaka, M. et al. Neurons expressing relaxin 3/INSL 7 in the nucleus incertus respond to stress. *Eur. J. Neurosci.* **21**, 1659–1670 (2005).
29. Banerjee, A., Shen, P. J., Ma, S., Bathgate, R. A. & Gundlach, A. L. Swim stress excitation of nucleus incertus and rapid induction of relaxin-3 expression via CRF1 activation. *Neuropharmacology* **58**, 145–155 (2010).
30. Ryan, P. J., Krstew, E. V., Sarwar, M., Gundlach, A. L. & Lawrence, A. J. Relaxin-3 mRNA levels in nucleus incertus correlate with alcohol and sucrose intake in rats. *Drug Alcohol Depend.* **140**, 8–16 (2014).
31. Walker, L. C. et al. Nucleus incertus corticotrophin-releasing factor 1 receptor signalling regulates alcohol seeking in rats. *Addict. Biol.* **22**, 1641–1654 (2017).
32. Kumar, J. R. et al. Relaxin the brain: a case for targeting the nucleus incertus network and relaxin-3/RXFP3 system in neuropsychiatric disorders. *Br. J. Pharmacol.* **174**, 1061–1076 (2017).
33. Ryan, P. J. et al. Central relaxin-3 receptor (RXFP3) activation decreases anxiety- and depressive-like behaviours in the rat. *Behav. Brain Res.* **244**, 142–151 (2013).
34. Lawther, A. J. et al. Anxiogenic drug administration and elevated plus-maze exposure in rats activate populations of relaxin-3 neurons in the nucleus incertus and serotonergic neurons in the dorsal raphe nucleus. *Neuroscience* **303**, 270–284 (2015).
35. Szonyi, A. et al. Brainstem nucleus incertus controls contextual memory formation. *Science* **364**, eaaw0445 (2019).
36. Pereira, C. W. et al. Electrolytic lesion of the nucleus incertus retards extinction of auditory conditioned fear. *Behav. Brain Res.* **247**, 201–210 (2013).
37. Marino, R. A. M. et al. Control of food approach and eating by a GABAergic projection from lateral hypothalamus to dorsal pons. *Proc. Natl Acad. Sci. USA* **117**, 8611–8615 (2020).
38. Hao, S. et al. The lateral hypothalamic and BNST GABAergic projections to the anterior ventrolateral periaqueductal gray regulate feeding. *Cell Rep.* **28**, 616–624.e615 (2019).
39. Nieh, E. H. et al. Decoding neural circuits that control compulsive sucrose seeking. *Cell* **160**, 528–541 (2015).
40. Cassidy, R. M. et al. A lateral hypothalamus to basal forebrain neurocircuit promotes feeding by suppressing responses to anxiogenic environmental cues. *Sci. Adv.* **5**, eaav1640 (2019).
41. Sakurai, T. The neural circuit of orexin (hypocretin): maintaining sleep and wakefulness. *Nat. Rev. Neurosci.* **8**, 171–181 (2007).
42. Petrovich, G. D. Lateral hypothalamus as a motivation-cognition interface in the control of feeding behavior. *Front. Syst. Neurosci.* **12**, 14 (2018).
43. Ryan, P. J., Ma, S., Olucha-Bordonau, F. E. & Gundlach, A. L. Nucleus incertus—an emerging modulatory role in arousal, stress and memory. *Neurosci. Biobehav. Rev.* **35**, 1326–1341 (2011).
44. Martínez-Bellver, S. et al. Regular theta-firing neurons in the nucleus incertus during sustained hippocampal activation. *Eur. J. Neurosci.* **41**, 1049–1067 (2015).
45. Cheron, G., Saussez, S., Gerrits, N. & Godaux, E. Existence in the nucleus incertus of the cat of horizontal-eye-movement-related neurons projecting to the cerebellar flocculus. *J. Neurophysiol.* **74**, 1367–1372 (1995).
46. Ma, S., Blasiak, A., Olucha-Bordonau, F. E., Verberne, A. J. M. & Gundlach, A. L. Heterogeneous responses of nucleus incertus neurons to corticotrophin-releasing factor and coherent activity with hippocampal theta rhythm in the rat. *J. Physiol.* **591**, 3981–4001 (2013).
47. Ma, S., Smith, C. M., Blasiak, A. & Gundlach, A. L. Distribution, physiology and pharmacology of relaxin-3/RXFP3 systems in brain. *Br. J. Pharmacol.* **174**, 1034–1048 (2017).
48. Bakshi, V. P., Newman, S. M., Smith-Roe, S., Jochman, K. A. & Kalin, N. H. Stimulation of lateral septum CRF2 receptors promotes anorexia and stress-like behaviors: functional homology to CRF1 receptors in basolateral amygdala. *J. Neurosci.* **27**, 10568–10577 (2007).
49. Qu, N. et al. A POMC-originated circuit regulates stress-induced hypophagia, depression, and anhedonia. *Mol. Psychiatry* **25**, 1006–1021 (2020).
50. Gozzi, A. et al. A neural switch for active and passive fear. *Neuron* **67**, 656–666 (2010).
51. Smith, C. M., Hosken, I. T., Sutton, S. W., Lawrence, A. J. & Gundlach, A. L. Relaxin-3 null mutation mice display a circadian hypoactivity phenotype. *Genes Brain Behav.* **11**, 94–104 (2012).
52. Hosken, I. T., Sutton, S. W., Smith, C. M. & Gundlach, A. L. Relaxin-3 receptor (Rxfp3) gene knockout mice display reduced running wheel activity: implications for role of relaxin-3/RXFP3 signalling in sustained arousal. *Behav. Brain Res.* **278**, 167–175 (2015).
53. Ma, S. & Gundlach, A. L. Ascending control of arousal and motivation: role of nucleus incertus and its peptide neuromodulators in behavioural responses to stress. *J. Neuroendocrinol.* **27**, 457–467 (2015).
54. Fanselow, M. S. Conditioned and unconditional components of post-shock freezing. *Pavlov. J. Biol. Sci.* **15**, 177–182 (1980).
55. Blair, H. T., Cho, J. W. & Sharp, P. E. Role of the lateral mammillary nucleus in the rat head direction circuit: a combined single unit recording and lesion study. *Neuron* **22**, U8–U8 (1999).
56. Vann, S. D. & Aggleton, J. P. The mammillary bodies: two memory systems in one? *Nat. Rev. Neurosci.* **5**, 35–44 (2004).
57. Vann, S. D. A role for the head-direction system in geometric learning. *Behav. Brain Res.* **224**, 201–206 (2011).
58. Vann, S. D. Transient spatial deficit associated with bilateral lesions of the lateral mammillary nuclei. *Eur. J. Neurosci.* **21**, 820–824 (2005).
59. Huang, W. C. et al. Lateral mammillary body neurons in mouse brain are disproportionately vulnerable in Alzheimer’s disease. *Sci. Transl. Med.* **15**, eabq1019 (2023).
60. Kania, A. et al. Inhibition of oxytocin and vasopressin neuron activity in rat hypothalamic paraventricular nucleus by relaxin-3-RXFP3 signalling. *J. Physiol.* **595**, 3425–3447 (2017).
61. Kania, A. et al. RLN3/RXFP3 signaling in the PVN inhibits magno-cellular neurons via M-like current activation and contributes to binge eating behavior. *J. Neurosci.* **40**, 5362–5375 (2020).
62. Ch’ng, S. S. et al. Characterization of the relaxin family peptide receptor 3 system in the mouse bed nucleus of the stria terminalis. *J. Comp. Neurol.* **527**, 2615–2633 (2019).

63. Cowley, M. A. et al. The distribution and mechanism of action of ghrelin in the CNS demonstrates a novel hypothalamic circuit regulating energy homeostasis. *Neuron* **37**, 649–661 (2003).
64. Betley, J. N. et al. Neurons for hunger and thirst transmit a negative-valence teaching signal. *Nature* **521**, 180 (2015).
65. Berrios, J. et al. Food cue regulation of AGRP hunger neurons guides learning. *Nature* **595**, 695 (2021).
66. Chen, Y. M., Lin, Y. C., Kuo, T. W. & Knight, Z. A. Sensory detection of food rapidly modulates arcuate feeding circuits. *Cell* **160**, 829–841 (2015).
67. Bauer, E. P. Sex differences in fear responses: neural circuits. *Neuropharmacology* **222**, 109298 (2023).
68. Toufexis, D. J., Myers, K. M., Bowser, M. E. & Davis, M. Estrogen disrupts the inhibition of fear in female rats, possibly through the antagonistic effects of estrogen receptor α (ER α) and ER β . *J. Neurosci.* **27**, 9729–9735 (2007).
69. Xu, Y. & Lopez, M. Central regulation of energy metabolism by estrogens. *Mol. Metab.* **15**, 104–115 (2018).
70. Rivera, H. M. & Stincic, T. L. Estradiol and the control of feeding behavior. *Steroids* **133**, 44–52 (2018).
71. Calvigioni, D. et al. Esr1⁺ hypothalamic-habenula neurons shape aversive states. *Nat. Neurosci.* **26**, 1245–1255 (2023).
72. Mystkowski, P. et al. Hypothalamic melanin-concentrating hormone and estrogen-induced weight loss. *J. Neurosci.* **20**, 8637–8642 (2000).
73. de Avila, C. et al. Estrous cycle modulation of feeding and relaxin-3/Rxrp3 mRNA expression: implications for estradiol action. *Neuroendocrinology* **111**, 1201–1218 (2021).
74. Yu, X. D. et al. Distinct serotonergic pathways to the amygdala underlie separate behavioral features of anxiety. *Nat. Neurosci.* **25**, 1651 (2022).
75. Kim, C. K. et al. Simultaneous fast measurement of circuit dynamics at multiple sites across the mammalian brain. *Nat. Methods* **13**, 325–328 (2016).

Acknowledgements

We are grateful to the Core Facilities of the Zhejiang University Institute of Neuroscience for technical assistance. This work was supported by the STI 2030-Major Projects (2021ZD0202702 and 2021ZD0202700 to X.M.L.), Major Program of the National Natural Science Foundation of China (82090031 and 82090030 to X.M.L.), National Natural Science Foundation of China (31900723 to Q.W. and 82001186 to H.W.), China Postdoctoral Science Foundation (2019TQ0278 to Q.W.), Young Elite Scientist Sponsorship Program by the China Association for Science and Technology (YESS20200014 to H.W.), and grants from Nanhu Brain-computer Interface Institute (010904005 to H.W.).

Author contributions

Q.W., H.W., and X.M.L. initiated and designed the research and wrote the manuscript. Q.W. and R.Y.S. performed all experiments and analyzed the results. J.X.H., Y.H.S., and C.Y.L. helped to collect and interpret the results. H.Q.H. contributed to the discussion of the results. X.M.L. supervised the entire project.

Competing interests

The authors declare no competing interests.

Additional information

Supplementary information The online version contains supplementary material available at <https://doi.org/10.1038/s41467-024-51983-6>.

Correspondence and requests for materials should be addressed to Hao Wang or Xiao-Ming Li.

Peer review information *Nature Communications* thanks Avishek Adhikari and the other, anonymous, reviewers for their contribution to the peer review of this work. A peer review file is available.

Reprints and permissions information is available at <http://www.nature.com/reprints>

Publisher's note Springer Nature remains neutral with regard to jurisdictional claims in published maps and institutional affiliations.

Open Access This article is licensed under a Creative Commons Attribution-NonCommercial-NoDerivatives 4.0 International License, which permits any non-commercial use, sharing, distribution and reproduction in any medium or format, as long as you give appropriate credit to the original author(s) and the source, provide a link to the Creative Commons licence, and indicate if you modified the licensed material. You do not have permission under this licence to share adapted material derived from this article or parts of it. The images or other third party material in this article are included in the article's Creative Commons licence, unless indicated otherwise in a credit line to the material. If material is not included in the article's Creative Commons licence and your intended use is not permitted by statutory regulation or exceeds the permitted use, you will need to obtain permission directly from the copyright holder. To view a copy of this licence, visit <http://creativecommons.org/licenses/by-nc-nd/4.0/>.

© The Author(s) 2024